The quantum marginal problem for symmetric states: applications to variational optimization, nonlocality and self-testing

Aloy, A.; Fadel, M.; Tura Brugués, J.

PAPER • OPEN ACCESS

The quantum marginal problem for symmetric states: applications to variational optimization, nonlocality and self-testing

To cite this article: Albert Aloy *et al* 2021 *New J. Phys.* **23** 033026

New Journal of Physics
The open access journal at the forefront of physics

Deutsche Physikalische Gesellschaft DPG
IOP Institute of Physics

Published in partnership with: Deutsche Physikalische Gesellschaft and the Institute of Physics

OPEN ACCESS

RECEIVED
3 November 2020

REVISED
25 January 2021

ACCEPTED FOR PUBLICATION
29 January 2021

PUBLISHED
15 March 2021

PAPER

The quantum marginal problem for symmetric states: applications to variational optimization, nonlocality and self-testing

Albert Aloy[1,*], Matteo Fadel[2] and Jordi Tura[3,4]

[1] ICFO-Institut de Ciencies Fotoniques, The Barcelona Institute of Science and Technology, 08860 Castelldefels (Barcelona), Spain
[2] Department of Physics, University of Basel, Klingelbergstrasse 82, 4056 Basel, Switzerland
[3] Max-Planck-Institut für Quantenoptik, Hans-Kopfermann-Straße 1, 85748 Garching, Germany
[4] Instituut-Lorentz, Universiteit Leiden, P.O. Box 9506, 2300 RA Leiden, The Netherlands
[*] Author to whom any correspondence should be addressed.

E-mail: albert.aloy@icfo.eu

Keywords: quantum marginal problem, symmetric states, variational optimization

Abstract

In this paper, we present a method to solve the quantum marginal problem for symmetric d-level systems. The method is built upon an efficient semi-definite program that uses the compatibility conditions of an m-body reduced density with a global n-body density matrix supported on the symmetric space. We illustrate the applicability of the method in central quantum information problems with several exemplary case studies. Namely, (i) a fast variational ansatz to optimize local Hamiltonians over symmetric states, (ii) a method to optimize symmetric, few-body Bell operators over symmetric states and (iii) a set of sufficient conditions to determine which symmetric states cannot be self-tested from few-body observables. As a by-product of our findings, we also provide a generic, analytical correspondence between arbitrary superpositions of n-qubit Dicke states and translationally-invariant diagonal matrix product states of bond dimension n.

1. Introduction

The quantum marginal problem (QMP) is ubiquitous not only in modern physics, but also in modern chemistry, where it is usually referred to as the n-representability problem [1]. The QMP can be stated as determining whether a set of reduced density matrices (RDMs) are compatible with a global wavefunction. The QMP arises naturally when computing physically important quantities such as the energy of a system or its entropy, as they often only depend on few particles. As an illustrative example, let us imagine one is interested in computing the ground energy of a k-local Hamiltonian $H = \sum_i H_i$, where each H_i acts nontrivially on at most k particles. The solution to this problem is $\langle\psi|H|\psi\rangle$, where $|\psi\rangle$ is an eigenvector of H with lowest corresponding eigenvalue. Unfortunately, the amount of computational resources to describe $|\psi\rangle$ grows, in general, exponentially with the system size, rendering this approach impractical. Alternatively, one can exploit the fact that H is a sum of much simpler terms, and compute instead $\langle\psi|H|\psi\rangle = \sum_i \mathrm{Tr}[H_i\rho_i]$, where each ρ_i is the reduced density matrix of $|\psi\rangle\langle\psi|$ on the particles H_i acts upon. The latter formulation, however, only appears to circumvent the exponential cost of describing $|\psi\rangle$. As a matter of fact, it actually comes at the cost of knowing the compatibility conditions of $\{\rho_i\}$ with a global state $|\psi\rangle\langle\psi|$.

Despite this apparent simplification, the QMP has challenged the physics and chemistry communities since the 60s and every nontrivial advance has already supposed a milestone in the field [2]. The QMP is strongly believed to be very hard, even for a quantum computer: it is complete for the complexity class quantum Merlin–Arthur (QMA) [3] which, roughly speaking, is the analogous of NP for a quantum computer. This may be not so surprising, since the k-local Hamiltonian problem itself is QMA-complete [4], even for $k = 2$ [5] or for quantum systems on a 1D geometry [6], and existing quantum algorithms take typically exponential time to solve it [7–10]. In spite of these intractability results, tremendous progress

has been achieved over the years in the QMP, even before the advent of the quantum information processing era [11–13].

A great deal of the aforementioned progress has centered onto the one-body RDM problem; i.e. determining if a set of one-body RDMs is compatible with a global (pure) state. Klyachko showed that in this case it is sufficient to characterize the QMP compatibility conditions solely from the eigenvalues of the one-body RDMs [2, 14]. For instance, the case of RDMs of a bipartite system is completely solved in terms of linear inequalities on the spectra [14], a rather surprising fact, since it is not obvious that compatible spectra form convex sets, let alone polytopes. This formalism has allowed for an elegant and mathematically tractable characterization, from which further results have stemmed [15, 16], for instance, in the context of witnessing genuinely multipartite entanglement from one-body RDMs [13].

The few-body QMP is encompassed with substantial additional challenges. First of all, the relevant information cannot be extracted solely from the eigenvalues of the RDMs, as it was the case on the one-body case. In the one-body case, the supports of different RDMs were necessarily disjoint; therefore, the action of local unitaries did not affect global compatibility and, in consequence, only the spectrum of the one-body RDMs was relevant. In the case that one considers few-body RDMs, their supports may intersect. Therefore, these must, at least, have the same reduced density matrix on the intersection of their supports. Despite the additional requirements, some progress has been made [17]: for instance, almost all four-partite pure states are determined by their two-body marginals [18]. The QMP has also been extensively studied under the bosonic and fermionic formalism [2, 12, 19–21]: there, one uses the assumption of the global pure state being either fully symmetric or antisymmetric and obtains conditions on the RDMs on a given subset of parties. These RDMs are all equal due to the symmetry of the global state. The QMP remains today a topic of intense research activity [22–24].

In this work we consider the following problem: given a reduced density matrix σ of m qudits, i.e. acting on the Hilbert space $(\mathbb{C}^d)^{\otimes m}$, is it compatible with a global density matrix ρ acting on the symmetric space of n qudits $\mathrm{Sym}(\mathbb{C}^d)^{\otimes n}$? Note that we denote the symmetric space as the subspace which is spanned by the Dicke states defined in section 2. We present the solution to this problem by analytically writing the compatibility conditions between σ and ρ and we show that they can be efficiently determined numerically as a feasibility semidefinite program (SdP) (section 3.1).

The core results of our work can be summarized as follows:

- We give the analytical conditions for any m-qudit RDM to be compatible with a larger n-qudit symmetric state
- We show how these compatibility conditions can be efficiently solved (polynomially in n, with degree $d-1$) via a SDP, thus enabling fast optimization over symmetric states

Our results can be seen as a solution to the N-representability problem for bosons in first quantization; i.e. for spin systems of identical, but distinguishable particles [25]. The N-representability problem also exists for bosons in second quantization, but there it was shown to be QMA-hard [26], mainly because the scaling that is taken is that the number of modes to be considered is proportional to the number of particles in the system. This yields an exponential scaling, whereas in our work the physical dimension of the qudits is fixed and independent of the number of particles in the system.

Our work has implications in several aspects of quantum information processing, as we show in subsequent sections with exemplary case studies. We show in section 3.3 how this provides a computationally undemanding variational approach to the ground state energy of any local Hamiltonian. We benchmark our results with different physical models, such as the Lipkin–Meshkov–Glick (LMG) from nuclear physics [27–29], an Ising chain with power-law interactions, and various XXZ chains with transverse and longitudinal magnetic fields (section 4.1). We further showcase how our method leads to a natural tool to optimize symmetric, few-body, Bell inequalities [30–32] and we apply our method to show the ground state of some XXZ one-dimensional model with 128 particles contains Bell correlations (section 4.2). In order to benchmark our results in large system sizes, we have also developed an analytical correspondence between pure symmetric states of n qubits and translationally invariant diagonal matrix product states (MPS) of bond dimension n (section 4.3) which may be of independent interest. Another exemplary case study that stems from our method may have implications on the self-testing of symmetric states from few-body correlators. Our method allows us to find sufficient conditions to certify which symmetric states cannot be self-tested from their marginals, by analyzing when the compatibility conditions do not lead to a unique solution (section 4.4). We discuss the implications of our results and discuss further research directions in section 5. The results presented in this manuscript are partly adapted from chapter 6 of the doctoral thesis in [33].

2. Preliminaries

Symmetric states constitute one of the most prominent classes of quantum states [34]. These are linear combinations of the so-called Dicke states, which arise naturally from the superradiance effect [35]. Dicke states and symmetric states have been successfully prepared in the laboratory in a plethora of systems, ranging from photons [36] to ultracold atoms [37, 38]. Their entanglement properties have been extensively studied [39–41]. Furthermore, device-independent (DI) self-testing protocols exist for Dicke states [42, 43], and symmetric states provide an advantage in quantum metrology [44]. Symmetric states are simple to describe, as their permutational invariance allows one to circumvent the exponential growth of the Hilbert space representability problem, therefore being confined to a subspace of the multipartite Hilbert space whose dimension scales only polynomially with n, with degree $d-1$: more precisely, we have $\dim_{\mathbb{C}} \mathrm{Sym}(\mathbb{C}^d)^{\otimes n} = \binom{n+d-1}{d-1}$.

Symmetric states are spanned by the Dicke states and, thus, can be conveniently represented by the so-called Dicke basis. In the case of n qubits, the Dicke states are typically denoted $|D_k^n\rangle$ and take the following form:

$$|D_k^n\rangle \propto \sum_{\tau\in\mathfrak{S}_n} \tau(|0\rangle^{\otimes(n-k)}|1\rangle^{\otimes k}), \tag{1}$$

where $\mathfrak{S}_n$ denotes the symmetric group (the group of permutations of n elements), and τ is a permutation acting on the different local Hilbert spaces.

For instance, the half-filled Dicke state of $n=4$ qubits has two excitations $k=2$, but they are delocalized among the different subsystems, in an equally-weighted coherent superposition of the same phase:

$$|D_2^4\rangle = \frac{1}{\sqrt{6}}\left(|0011\rangle + |0101\rangle + |0110\rangle + |1001\rangle + |1010\rangle + |1100\rangle\right). \tag{2}$$

The number of different terms in a qubit Dicke state of k excitations is given by the combinatorial expression $\binom{n}{k}$ and there are $n+1$ Dicke states for $d=2$.

In the general case of qudits, now one needs to specify how many $|1\rangle$ excitations there are, how many $|2\rangle$ excitations, etc. Hence, it is a natural choice to index Dicke states by partitions of n. For this purpose, whenever $\boldsymbol{\lambda} = (\lambda_i)_{i=0}^{d-1}$ be a vector with non-negative entries, then we denote $\boldsymbol{\lambda} \vdash n$ if $\boldsymbol{\lambda}$ is a partition of n in d elements, i.e. $\sum_{i=0}^{d-1}\lambda_i = n$. We will omit mentioning d whenever it is clear from the context. There are $\binom{n+d-1}{d-1}$ such partitions and a qudit Dicke state is denoted by $|D_{\boldsymbol{\lambda}}\rangle$, where

$$|D_{\boldsymbol{\lambda}}\rangle \propto \sum_{\tau\in\mathfrak{S}_n} \tau(|0\rangle^{\otimes\lambda_0} \otimes \cdots \otimes |d-1\rangle^{\otimes\lambda_{d-1}}). \tag{3}$$

The number of different terms in equation (3) is given by the multinomial combinatorial expression

$$\binom{n}{\boldsymbol{\lambda}} = \frac{n!}{\lambda_0!\ldots\lambda_{d-1}!}. \tag{4}$$

For the sake of a more compact notation, in the rest of this manuscript we will denote the qudit Dicke state $|D_{\lambda}\rangle$ simply as $|\boldsymbol{\lambda}\rangle$, since D is void of meaning.

3. Main result: the QMP for symmetric states

In this section we present our main results: first, in section 3.1 we derive a complete set of necessary and sufficient conditions for an m-qudit reduced density matrix to be compatible with a global n-qudit symmetric density matrix; second, in section 3.2 we show that, by means of the compatibility conditions from section 3.1, one can express the QMP for symmetric states as a feasibility problem which is efficiently solvable with semidefinite programming techniques; finally, in section 3.3 we illustrate how the solution from section 3.2 can be used as a variational ansatz, whose applications are further explored in section 4.

3.1. Compatibility conditions with a global symmetric state

Here we outline the fundamental building block of our work. We derive a set of necessary and sufficient conditions for compatibility of an m-qudit (symmetric) density matrix σ with a global n-qudit symmetric density matrix ρ.

Let us consider a quantum system of n qudits in the symmetric state ρ. Let us denote the components of ρ by $\rho^{\boldsymbol{\lambda}}_{\boldsymbol{\mu}}$, where $\boldsymbol{\lambda}, \boldsymbol{\mu} \vdash n$. Thus,

$$\rho = \sum_{\boldsymbol{\lambda},\boldsymbol{\mu}\vdash n} \rho^{\boldsymbol{\lambda}}_{\boldsymbol{\mu}} |\boldsymbol{\lambda}\rangle\langle\boldsymbol{\mu}|. \tag{5}$$

Our first goal is to find closed-form expressions, both in the computational and in the Dicke basis, that relates the matrix elements of ρ, with the matrix elements of its m-particle RDM. Note that, since ρ is symmetric, the choice of which $n-m$ subsystems to trace out plays no role.

Before stating theorem 1, we introduce the following notations. We define $[d] := \{0, \ldots, d-1\}$, and we shall use indices with an overhead arrow (e.g. $\vec{i}$) to denote matrix elements in the computational basis, as opposed to indices in boldface (e.g. $\boldsymbol{\lambda}$) that denote matrix elements in the Dicke basis. We recall once more that such boldface indices consist in partitions of n, and they are associated to the Dicke basis elements through equation (3).

Theorem 1. *Let ρ be a symmetric state of n qudits, and $m \leqslant n$. Let $\vec{i}, \vec{j} \in [d]^m$ and $\boldsymbol{\alpha}, \boldsymbol{\beta} \vdash m$, so that we define $\sigma := \mathrm{Tr}_{n-m}(\rho)$; i.e.*

$$\sigma = \sum_{\vec{i},\vec{j}\in[d]^m} \sigma^{\vec{i}}_{\vec{j}} |\vec{i}\rangle\langle\vec{j}| = \sum_{\boldsymbol{\alpha},\boldsymbol{\beta}\vdash m} \sigma^{\boldsymbol{\alpha}}_{\boldsymbol{\beta}} |\boldsymbol{\alpha}\rangle\langle\boldsymbol{\beta}|. \tag{6}$$

Then, we have the coefficients in the computational basis

$$\sigma^{\vec{i}}_{\vec{j}} = \sum_{\boldsymbol{\lambda},\boldsymbol{\mu}\vdash n} \rho^{\boldsymbol{\lambda}}_{\boldsymbol{\mu}} \sum_{\boldsymbol{\kappa}\vdash n-m} \frac{\binom{n-m}{\boldsymbol{\kappa}}}{\sqrt{\binom{n}{\boldsymbol{\lambda}}\binom{n}{\boldsymbol{\mu}}}} \delta(\boldsymbol{w}(\vec{i}) + \boldsymbol{\kappa} - \boldsymbol{\lambda}) \delta(\boldsymbol{w}(\vec{j}) + \boldsymbol{\kappa} - \boldsymbol{\mu}), \tag{7}$$

where $\delta(\boldsymbol{v}) = 1$ iff $\boldsymbol{v}$ is the zero vector and $\delta(\boldsymbol{v}) = 0$ otherwise. We have also defined the function $\boldsymbol{w}(\vec{i}) := (w_0(\vec{i}), \ldots, w_{d-1}(\vec{i}))$, with $w_k(\vec{i})$ counting how many coordinates of $\vec{i}$ are equal to $k \in [d]$ (for the details see appendix A), and the coefficients in the Dicke basis

$$\sigma^{\boldsymbol{\alpha}}_{\boldsymbol{\beta}} = \sum_{\boldsymbol{\lambda},\boldsymbol{\mu}\vdash n} \rho^{\boldsymbol{\lambda}}_{\boldsymbol{\mu}} \sum_{\boldsymbol{\kappa}\vdash n-m} \binom{n-m}{\boldsymbol{\kappa}} \sqrt{\frac{\binom{m}{\boldsymbol{\alpha}}\binom{m}{\boldsymbol{\beta}}}{\binom{n}{\boldsymbol{\lambda}}\binom{n}{\boldsymbol{\mu}}}} \delta(\boldsymbol{\alpha} + \boldsymbol{\kappa} - \boldsymbol{\lambda}) \delta(\boldsymbol{\beta} + \boldsymbol{\kappa} - \boldsymbol{\mu}). \tag{8}$$

A proof of theorem 1 can be found in appendix A. Note that equations (7) and (8) provide a set of compatibility conditions for all the elements of a reduced density matrix σ of m qudits to be compatible with a global (possibly mixed) symmetric state ρ of n qudits. Therefore, by also imposing the constraints for ρ to be a valid quantum state, i.e. $\rho \succeq 0$ & $\mathrm{Tr}(\rho) = 1$, then one has a complete set of necessary and sufficient compatibility conditions.

3.2. Efficient solution as a feasibility problem

In this section we describe an efficient solution to the QMP for symmetric states. In particular, we express the QMP for symmetric states as a feasibility problem by means of semidefinite programming (SDP) techniques. In appendix B a brief summary of SDP basic notions is included.

In particular, the complete set of compatibility conditions from section 3.1 makes it straightforward to write them down as an SDP that tests feasibility for an m-qudit RDM σ to be compatible with an n-qudit global symmetric state ρ:

$$\begin{aligned} &\min_{\rho} \ 0 \\ &\text{subject to } \rho \succeq 0, \mathrm{Tr}(\rho) = 1, \\ &\qquad \sum_{\boldsymbol{\lambda},\boldsymbol{\mu}\vdash n} \rho^{\boldsymbol{\lambda}}_{\boldsymbol{\mu}} a^{\boldsymbol{\lambda},\boldsymbol{\alpha}}_{\boldsymbol{\mu},\boldsymbol{\beta}} = \sigma^{\boldsymbol{\alpha}}_{\boldsymbol{\beta}} \quad \forall\, \boldsymbol{\alpha}, \boldsymbol{\beta} \vdash m, \end{aligned} \tag{9}$$

where the coefficients $a^{\boldsymbol{\lambda},\boldsymbol{\alpha}}_{\boldsymbol{\mu},\boldsymbol{\beta}}$ are defined to account for the compatibility conditions in equation (8) (similarly for equation (7)); namely,

$$a^{\boldsymbol{\lambda},\boldsymbol{\alpha}}_{\boldsymbol{\mu},\boldsymbol{\beta}} := \sum_{\boldsymbol{\kappa}\vdash n-m} \binom{n-m}{\boldsymbol{\kappa}} \sqrt{\frac{\binom{m}{\boldsymbol{\alpha}}\binom{m}{\boldsymbol{\beta}}}{\binom{n}{\boldsymbol{\lambda}}\binom{n}{\boldsymbol{\mu}}}} \delta(\boldsymbol{\alpha} + \boldsymbol{\kappa} - \boldsymbol{\lambda}) \delta(\boldsymbol{\beta} + \boldsymbol{\kappa} - \boldsymbol{\mu}). \tag{10}$$

Furthermore, by expressing $a^{\boldsymbol{\lambda},\boldsymbol{\alpha}}_{\boldsymbol{\mu},\boldsymbol{\beta}}$ as the entries of a matrix $A^{\boldsymbol{\alpha}}_{\boldsymbol{\beta}}$ indexed by $\boldsymbol{\lambda}$ and $\boldsymbol{\mu}$, the SDP equation (9) is automatically written in canonical form:

$$\begin{aligned} &\min_{\rho} \ \langle 0, \rho \rangle \\ &\text{subject to } \rho \succeq 0, \mathrm{Tr}(\rho) = 1, \\ &\qquad \langle A^{\boldsymbol{\alpha}}_{\boldsymbol{\beta}}, \rho \rangle = \sigma^{\boldsymbol{\alpha}}_{\boldsymbol{\beta}} \quad \forall\, \boldsymbol{\alpha}, \boldsymbol{\beta} \vdash m, \end{aligned} \tag{11}$$

where $\langle \cdot, \cdot \rangle$ denotes the Hilbert–Schmidt inner product.

Some comments are in order. First, let us start by noting that in the SDPs in equations (9) and (11) we are taking 0 as the objective function, thus expressing the SDPs as a feasibility problem, meaning that the only output from the SDP is the answer *feasible* or *infeasible*, depending on whether the feasible set of ρ is empty or not (cf appendix B for details). Therefore, when the SDP in equation (11) is feasible, then it is certified that σ admits an extension into a symmetric Dicke state ρ of n qudits (which is precisely the solution of that SDP). In section 4.4 we discuss the uniqueness of that solution.

Second, let us note that the free variables of ρ act as the decision variables to be optimized with the SDP technique. More precisely, the free variables from ρ can be seen as extra variables on the original problem, thus defining the set of feasible σ's as a projected spectrahedron (see e.g. section 5.6 of [45]). Since ρ acts in the symmetric subspace, the number of extra variables will be at most polynomial in the system size n with degree $d-1$, which makes the procedure efficient. Let us emphasize that the optimization is not directly carried over the whole symmetric space of ρ, since some entries of ρ are eliminated by the equality constraints in section 3.1.

Finally, let us comment on the purity of the compatible state ρ. One can easily combine our methodology with the algorithm in section 3.7 of [17] in order to obtain a pure global state ρ (if such a ρ exists for a given σ). In particular, the algorithm would need to iterate equation (11), where at each iteration one would keep the projector onto the highest eigenvalue subspace of the obtained solution ρ until convergence to a rank-1 projector, thus attaining purity (which in the average case happens in less than 4 iterations [17]).

3.3. Variational ansatz

We can now easily modify the SDP in equation (11) to optimize any linear functional H on ρ, while maintaining compatibility over a given marginal state σ. This is done by considering the following SDP:

$$\begin{aligned} &\min \ \langle H, \rho \rangle \\ &\text{s.t. } \rho \succeq 0 \\ &\langle A^{\boldsymbol{\alpha}}_{\boldsymbol{\beta}}, \rho \rangle = \sigma^{\boldsymbol{\alpha}}_{\boldsymbol{\beta}} \quad \forall\, \boldsymbol{\alpha}, \boldsymbol{\beta} \vdash m. \end{aligned} \tag{12}$$

The most interesting case arises when such a functional can be expressed as a sum of terms with support on, at most, m qudits. This includes many cases of physical interest, such as Hamiltonians or Bell operators composed of, at most, m-body interactions/correlators. In this case, let us denote $H = \sum_i H_i$. Then, $\langle H, \rho \rangle$ can be expressed as a linear combination of terms of the form $\langle H_i, \sigma \rangle$, namely:

$$\begin{aligned} &\min \ \sum_i \langle H_i, \sigma \rangle \\ &\text{s.t. } \rho \succeq 0 \\ &\langle A^{\boldsymbol{\alpha}}_{\boldsymbol{\beta}}, \rho \rangle = \sigma^{\boldsymbol{\alpha}}_{\boldsymbol{\beta}} \quad \forall\, \boldsymbol{\alpha}, \boldsymbol{\beta} \vdash m. \end{aligned} \tag{13}$$

Note that, while in section 3.2 we were interested in the case where σ is given, in equation (13) both ρ and σ are treated as positive-semidefinite variables. The positive-semidefiniteness of σ is automatically implied by that of ρ. In fact, σ can be completely removed from equation (13) and embedded into the objective function; however we keep it in this form for clarity of exposition. The form of equation (13) is thus useful to optimize a functional H that depends only on the marginal information contained in the reduced states, while keeping compatibility with a global symmetric state. Recall that the size of ρ depends polynomially on n, with a degree $d-1$, so that this procedure is efficient for systems of qudits of large n and fixed d.

4. Some applications

The aim of this section is to illustrate several applications in various, apparently uncorrelated, problems in quantum information, all of which have deep roots in the QMP.

In section 4.1 (and appendix C) we apply equation (13) to benchmark our method as a variational ansatz to find a fast, upper bound, to the ground state energy and, in some cases, to well approximate the

ground state of several paradigmatic Hamiltonians. In section 4.2 we adapt our method to optimize Bell functionals composed of symmetric, few-body observables. In section 4.3 we provide a method to approximate any n-qubit Dicke state with a translationally-invariant (TI) diagonal MPS of bond dimension n. Finally, in section 4.4 we show how our method can be used to show which symmetric states cannot be self-tested from few-body marginals.

4.1. Benchmarking the variational ansatz

Here we consider some Hamiltonians of exemplary spin models, complemented in appendix C, in order to benchmark the performance of the variational ansatz presented in section 3.3. In particular, we consider: the LMG model (section 4.1.1) and one of its SU(3) variations (appendix C.4); an Ising chain under a transverse field with power-law decaying interactions (section 4.1.2) and with nearest-neighbours interactions (appendix C.1); and the XXZ chain under a transverse field (appendix C.2) and the ferromagnetic (FM) XXZ with longitudinal magnetic field and periodic boundary conditions (appendix C.3). Furthermore, for the Ising chain with power-law decaying interactions model we provide in section 4.1.3 the runtime and estimated resources consumed by our method, compared to density matrix renormalization group (DMRG) as a benchmark.

The variational ansatz approximates the ground state and energy of an m-local Hamiltonian by an m-qudit RDM (denoted m-RDM for short) compatible with a global many-body symmetric state. Therefore, we expect the variational ansatz to provide a good approximation when the coupling interactions are similar between all pairs and to provide exact results when the ground state lies in the symmetric space.

4.1.1. Lipkin–Meshkov–Glick model

Let us start by considering a spin model for which our variational method (VM) recovers the ground state exactly. We picked as an example the LMG model [27–29], which involves long-range interactions that result in ground states that are symmetric under any permutation of the particles. The LMG model was originally proposed in nuclear physics to describe phase transitions in nuclei. However, nowadays it also serves to describe e.g. two-mode Bose–Einstein condensates experiments, since it captures the physics of interacting bosons in a double-well trapping potential. Furthermore, in its isotropic version, the ground states of the LMG model are pure Dicke states, which have been shown to display Bell correlations [30, 32, 46]. The phase transitions of the general model are also well understood [47]. Analytical expressions for the ground state entanglement entropy have been found [48–50] and exact solutions of the model are known [51–53], which we use here to benchmark our method.

In particular, we consider the following LMG Hamiltonian which describes a set of n spin-1/2 particles with anisotropic long-range interactions under an external transverse magnetic field h:

$$\mathcal{H} = -\frac{\lambda}{n}\sum_{i<j}\left(\sigma_x^{(i)}\sigma_x^{(j)} + \gamma\sigma_y^{(i)}\sigma_y^{(j)}\right) - h\sum_{i=1}^{n}\sigma_z^{(i)}, \tag{14}$$

where $\sigma_k^{(i)}$ denotes the Pauli matrix in position i and direction k, $\lambda > 0$ correspond to FM interactions, $\lambda < 0$ correspond to anti-ferromagnetic (AFM) interactions, and γ marks the anisotropy in the coupling terms, with $\gamma = 1$ being the isotropic case.

By adapting the SDP optimization problem in equation (13), we can use the 2-RDM compatibility constraints to approximate its ground state by means of SDP. In particular, the optimization problem to find the best approximation within the variational ansatz can be reduced to the following SDP:

$$\begin{aligned} &\min\ \mathrm{Tr}\left(\tilde{\mathcal{H}}\sigma\right) \\ &\text{s.t. } \rho \succeq 0 \\ &\langle A_\beta^\alpha, \rho\rangle = \sigma_\beta^\alpha \quad \forall\, \boldsymbol{\alpha}, \boldsymbol{\beta} \vdash m, \end{aligned} \tag{15}$$

where we emphasize that $\tilde{\mathcal{H}} := -\binom{n}{2}\frac{\lambda}{n}\left(\sigma_x\otimes\sigma_x + \gamma\sigma_y\otimes\sigma_y\right) - nh\left(\sigma_z\otimes\mathbb{1} + \mathbb{1}\otimes\sigma_z\right)/2$ is now an effective two-body Hamiltonian.

In figure 1 we show that the ground state energy of the model we considered is faithfully recovered using our VM.

We note that this method unlocks the possibility to have access to an efficient description of the n-qubit state (given in the symmetric basis equation (8)), since it is a matrix of size $(m+1)\times(m+1)$. This, in turn, allows to obtain any associated m-RDM $\forall 1 \leqslant m \leqslant n$. This enables us to study the method against extensive quantities such as entropy, since it is now easy to obtain the m-block size entanglement entropy $\mathcal{S}_{m,n} = -\sum_{i=0}^{m} p_i \log_2 p_i$ by finding the eigenvalues p_i of the m-RDM [47]. In figure 1 we have used such a procedure to obtain the half-system entanglement entropy. The method reproduces the features of the LMG model phase diagram, as expected.

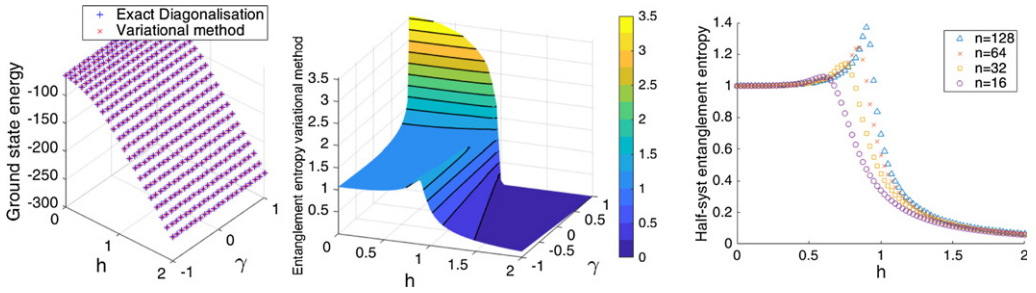

Figure 1. Numerical results for the LMG Hamiltonian (14) with $h = \lambda = 1$. Left: the VM faithfully reproduces the ground state energy of the LMG model for $n = 128$. Up to numerical error ($\sim 10^{-14}$ using SeDuMi [54]) the values coincide. Center: always for $n = 128$, we use the RDM compatibility constraints to obtain the half-system RDM from the ground state found by the VM. This enables us to compute the entanglement entropy, and to characterize the phase diagram of the model [47]. Right: half-system entanglement entropy for $\gamma = 0$ and different values of n obtained from the VM using the RDM compatibility constraints in the symmetric basis. For $\gamma \neq 1$, one can appreciate the anomaly in $h = 1$ as we increase n, which becomes a critical point in the asymptotic limit.

In order to illustrate that the VM can easily be implemented to d-level systems with local Hilbert space of dimension $d > 2$, in appendix C.4 we consider the three-orbital LMG Hamiltonian for which we obtain similar results as the ones presented in this section.

4.1.2. Ising chain with variable-range interactions under a transverse field

As a second example, we consider the Ising model with variable-range interactions in a transverse field. The tuneable interaction range allows us to explore how our VM performs as the range of interactions decreases from the infinite-range case (equivalent to the LMG model) to the nearest-neighbour case. In particular, we consider the following Hamiltonian for an Ising chain with decaying power-law interactions:

$$\mathcal{H} = \sin(\theta)\sum_{i<j} J_{ij}\sigma_z^{(i)}\sigma_z^{(j)} + \cos(\theta)\sum_{i=1}^{n}\sigma_x^{(i)}, \tag{16}$$

where $J_{ij} = |i-j|^{-\alpha}$, the parameter α tunes the range of interactions, and $\theta > 0$ ($\theta < 0$) results in AFM (FM) interactions. We note that in the limit $\alpha \to 0$ all pairs interact with the same strength [55], whereas in the other extreme $\alpha \to \infty$ we have interactions only between nearest neighbors. The phase diagram for this model has been extensively characterised [56–58]. In particular, for $\alpha > 0$ the model exhibits three phases: an ordered FM phase for $-\pi/2 \leqslant \theta < \theta_c^-(\alpha)$; a disordered paramagnetic phase for $\theta_c^-(\alpha) < \theta < \theta_c^+(\alpha)$; and an ordered AFM phase for $\theta_c^+(\alpha) < \theta \leqslant \pi/2$. Notably, such a model has also been shown to display Bell correlations at the critical points for the FM couplings [59].

In order to construct the VM for equation (16), we consider the SDP in equation (15) with the effective Hamiltonian $\tilde{\mathcal{H}} := J\ \sin(\theta)\sigma_z \otimes \sigma_z + n\ \cos(\theta)(\sigma_x \otimes \mathbb{1} + \mathbb{1} \otimes \sigma_x)/2$, where $J := \sum_{i<j} J_{ij}$.

In figure 2 we compare the ground states obtained using our VM with those obtained from exact diagonalisation (ED), in terms of relative energy and fidelity. To compare the ground state energies we look at their ratio, $E_0^{\mathrm{VM}}/E_0^{\mathrm{ED}}$. For this, a few comments are in order: first of all, note that the ground state energy is negative and sufficiently far from zero to constitute a good approximation of $1-\delta$, where δ is the relative error. Second, we have chosen the ratio as a figure of merit, instead of the relative error, as it gives a better visual comparison with the fidelity also plotted in figure 2. To compute the ground state fidelity we use the definition $F(\rho_{\mathrm{ED}}, \rho_{\mathrm{VM}}) := \left(\mathrm{Tr}\sqrt{\sqrt{\rho_{\mathrm{ED}}}\rho_{\mathrm{VM}}\sqrt{\rho_{\mathrm{ED}}}}\right)^2$. For this model we expect that the analytical solutions for the long-range interaction regime are well approximated by the one for the LMG model, where our VM yields exact results. However, in the transition from $\alpha \gg 1$ to $\alpha \simeq 0$ the quality of the approximation is *a priori* not so clear. In figure 2 it can be appreciated that for $\alpha > 0$ the method fails to capture the AFM phase $\theta_c^+(\alpha) < \theta$, eventually yielding fidelities close to zero. On the other hand, for values $\theta < \theta_c^+(\alpha)$ the method provides a good approximation, even though for sufficiently large α the method is less accurate near the critical point θ_c^-.

In figure 3 we compare half-system entanglement entropies obtained from the VM and ED. As expected, we observe a discrepancy in the AFM phase, because of the little overlap between the ground state and the symmetric space in that region. Interestingly, we see from figure 3 that in the FM regime one can use the VM (without ED) to approximate its phase transition (between paramagnetic and FM) for different number of particles, and extrapolate its asymptotic limit. Such an approximation naturally works better as the range of interactions increases.

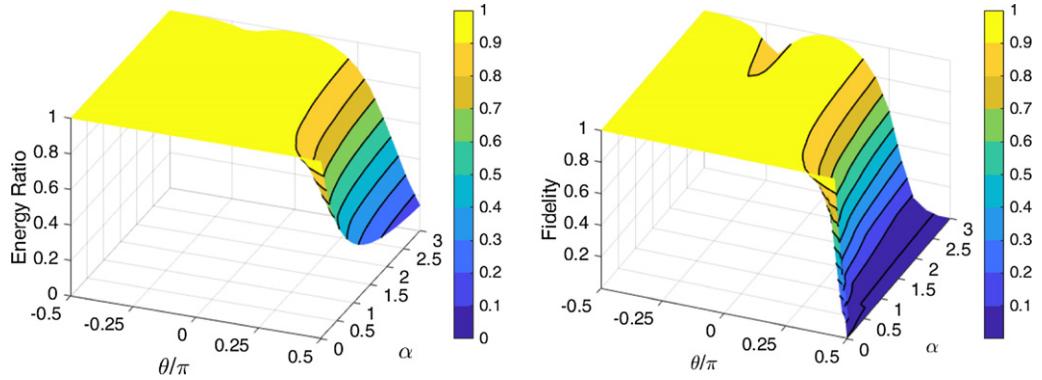

Figure 2. Numerical results for the Ising Hamiltonian (16) with $n = 10$, compared to exact diagonalization. Left: energy ratio, right: ground state fidelity. As expected, the case $\alpha = 0$ is faithfully recovered by the VM. However, we observe that as the value of α increases (the range of interaction decreases) the VM fails to capture the AFM phase for which the fidelity eventually drops to zero. The ground state energy and fidelity in the FM and paramagnetic phases are well approximated, although for large values of α there is a little discrepancy near the critical points $\theta \approx \theta_c^-(\alpha)$.

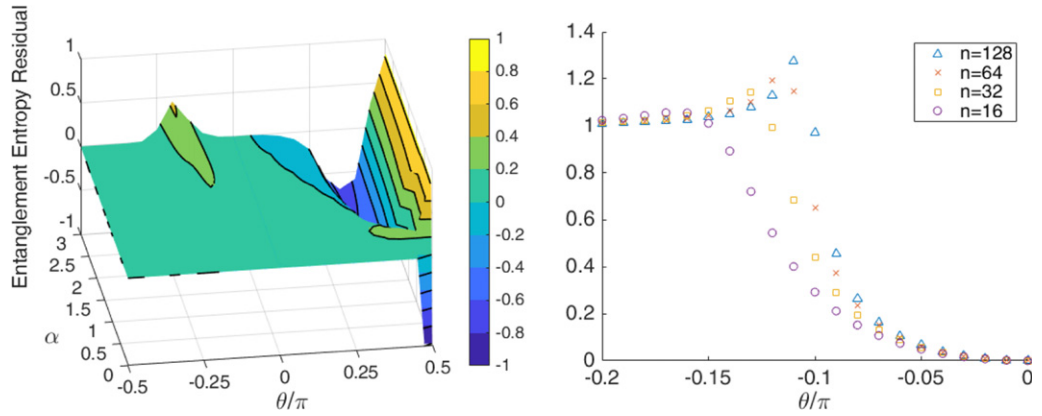

Figure 3. Numerical results for the Ising Hamiltonian (16) with $n = 10$. Left: half-system entanglement entropy residual obtained from comparing VM with ED (a value of 0 indicates an exact result). Although the paramagnetic to AFM phase transition is not reproduced by the VM, one observes that the transition from FM to paramagnetic is well approximated by looking at the discrepancies for values of $\alpha \gtrsim 1.5$. Right: half-system entanglement entropy for $\alpha = 2$. Note that the transition from FM to paramagnetic manifest itself in the vicinity of $\theta \simeq -0.1\pi$ for $n = 10$. From this observation we conjecture that our VM can be used to extrapolate some critical points where phase transitions occurs. We remark that the ED has not been used in this case and that the behavior observed arises from the VM alone.

The VM has the potential to identify a phase transition in the model due to the following argument: one might expect that in many cases of interest, and for a finite number of particles, the sudden change in nature (e.g. symmetry) of the ground state is actually 'smeared' rather smoothly around the critical point. Therefore, everywhere around this point the ground state may still have some overlap with the symmetric space, which is the one considered by our VM. The numerical evidence presented in figure 3 supports this conjecture.

Let us finish this section by mentioning that in appendix C.1 we have examined the VM performance in the particular case of nearest-neighbours interactions (i.e. $\alpha \to \infty$). Furthermore, since the nearest-neighbours case is solvable by equivalently describing the model as a system of free fermions, in appendices C.2 and C.3 we explore the performance of our variational ansatz beyond the free fermion scope by considering various XXZ chains with transverse and magnetic fields.

4.1.3. Benchmarking performance with existing methods

One of the most appealing features of the VM proposed here is its ability to yield results for large system sizes with very modest time and memory requirements (and, consequently, energy consumption). Indeed, since the computations take place in the symmetric space, its dimension grows only polynomially with the system size. In particular, it is linear for qubits, quadratic for qutrits, etc. In the previous sections we have argued that the method yields results that capture traces of some quantities of physical interest. Therefore, it can be a good candidate to a first order exploration before trying more numerically-intensive results. To

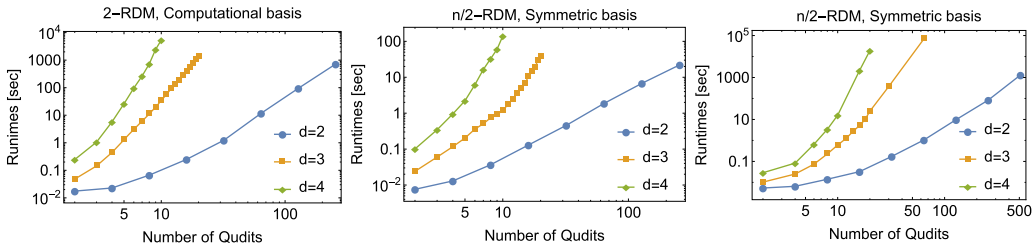

Figure 4. Runtimes observed in order to preallocate the 2-RDMs and $n/2$-RDMs compatibility constraints in the computational and symmetric basis. Apart from the memory storage advantage, it is observed that the symmetric spaces offers a significant advantage also in runtimes. The computations have been carried out on a 64-bit operating system with 32 GB ram and a 3.70 GHz processor. No parallelization has been used, which can be easily be implemented, significantly speeding up the process. The runtimes might slightly vary at each run and are not meant to be taken as exact, but as an illustration of their order.

make this comparison quantitative, we here benchmark the computational requirements of the method with other existing techniques.

In this section we briefly comment on the time, memory and energy consumption devoted to the variational ansatz. The runtime of the VM can be split in two steps: (1) to precompute the A matrices in equation (11) for a fixed n, m and d and (2) to load and solve the SDP. The most expensive task, both in time and memory, is to compute the compatibility constraints. Hence, in order to agilitate the process, one would first preallocate and store the compatibility constraints for a fixed number of particles n, of local Hilbert space dimension d and with RDMs of size m. Then, once the compatibility constraints are preallocated, one can scan the phase diagram of the desired parametrized Hamiltonian model just by loading the compatibility constraints and proceeding to solve the corresponding SDP.

In figure 4 we present a representative sample of the computing runtimes we have observed in order to preallocate the compatibility constraints of the 2-RDMs and half-system $n/2$-RDMs for different number of particles n and different local Hilbert space dimensions d. We have considered the 2-RDMs compatibility constraints case both in the computational basis (equation (7)) and the symmetric basis (equation (8)). Apart from requiring less memory, one observes a clear advantage in runtime when obtaining the compatibility constraints directly in the symmetric basis, as expected. Therefore, for the VM it is desirable to project the effective Hamiltonian onto the symmetric subspace. For the $n/2$-RDMs case, we have considered only the symmetric representation which decreases the memory storage limitations in order to find, for instance, the half-system entanglement entropies. An additional comment is in order: for a constant value of d, note that the multinomial coefficients in equation (7) or equation (8) do not require a full expansion of the factorials, but there exist closed analytical formulas for them (see e.g. [32]). This has been taken into consideration in our calculations. Furthermore, it is desirable to apply such closed expressions, not only for speed, but more importantly for numerical stability issues (quotients of factorials of large numbers may give problems in floating-point arithmetic if these numbers are of the order of $\sim$100).

In figure 5 we present some of the computing runtimes in order to load the constraints and solve the SDP for the Ising chain with decaying power-law interactions previously considered in section 4.1.2. We have considered the constraints and effective Hamiltonian in the symmetric basis, and in order to solve the SDP we have set the solver SDPT3 [60] to its maximal precision providing a numerical error up to $\mathcal{O}(10^{-14})$ when the variational ansatz can reach the exact solution. We have carried out the comparison with the solution provided by DMRG. In order to find the fidelity between the DMRG solution and the VM solution, we have used the auxiliary results developed in section 4.3 in order to represent the VM solution as a translationally invariant diagonal MPS.

Let us finish this section by remarking that, in order to compute the fidelity of our variational solution with respect to the exact one, the most straightforward way we have considered is to contract the MPS representation of the ground state with the solution of the VM. However, the latter is not given in a MPS form and it therefore has to be converted in a MPS form. In order to do so, we need to establish a correspondence between arbitrary superpositions of Dicke states and MPS. To the best of our knowledge, in general such a correspondence has not been established before, and this result may be of independent interest. Therefore, we have devoted a full section (section 4.3) to it.

4.2. Bell non-local correlations

The proposed variational ansatz is also convenient to investigate Bell non-local correlations in many-body systems. The permutational symmetry naturally synergizes with the so-called two-body permutation

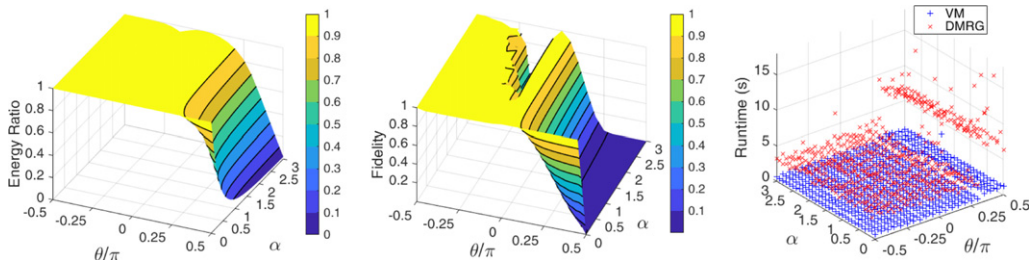

Figure 5. Numerical results of the VM for the Ising Hamiltonian (16) with $n = 64$, compared with DMRG. The DMRG algorithm follows [59, 61, 62] increasing the bond dimension up to 20. Left and center: energy ratio and fidelity of the VM solution with respect to the DMRG solution. In order to compute the fidelity we use the result in section 4.3 to transform the symmetric basis representation of the VM solution into a MPS representation. Right: runtimes comparison to achieve convergence with DMRG and VM method. The VM is significantly faster, making it a good candidate for a first rough exploration of large phase diagrams, and to upper bound ground state energies. Note that runtimes might slightly vary at each run. The total runtimes are 525.04 s (1 s preallocation) for the VM and 2854.25 s for the DMRG. With a power consumption of 425 W in our workstation, amounts to an environmental impact of around 18 g vs 100 g of CO_2 into the atmosphere for the VM vs the DMRG methods (we have taken the 0.296 EU coefficient of kW h to kg of CO_2 given by the European Environment Agency for 2016). We remark that the DMRG is an extremely optimized and efficient method that cannot be applied beyond 1 geometric dimension. In these cases, the benchmark with existing methods would be separated by even more orders of magnitude.

invariant Bell inequalities (PIBIs) presented in [30]. This type of Bell inequalities involve at most two-body correlation functions, and some of them are violated by symmetric states [32]. One can now consider two approaches: on the one hand, to obtain the quantum state that gives the maximal violation of such equalities within the variational ansatz. On the other hand, to find quantum states that also have Bell correlations by using the VM to approximate the ground state of a many-body Hamiltonian. In the latter case, the Hamiltonian considered needs not correspond to the Bell operator [46]. It is worth mentioning that the measurement settings might need to be optimized in order to increase the visibility of the Bell correlations.

4.2.1. Optimizing permutationally invariant two-body Bell inequalities

We first focus on two particular classes of two-body PIBIs. These inequalities satisfy the following condition for all correlations that can be described under local-realism assumptions (meaning that their violation signals the presence of non-local correlations, the so-called *nonlocality* [63]):

$$-2\mathcal{S}_0 + \frac{1}{2}\mathcal{S}_{00} - \mathcal{S}_{01} + \frac{1}{2}\mathcal{S}_{11} \geqslant -2n \tag{17}$$

and

$$(n \bmod 2)(n-1)(n\mathcal{S}_0 + \mathcal{S}_1) + \binom{n}{2}\mathcal{S}_{00} + n\mathcal{S}_{01} - \mathcal{S}_{11} \geqslant \binom{n}{2}(n+2+n \bmod 2), \tag{18}$$

where $\mathcal{S}_k = \sum_{i=1}^{n}\langle \mathcal{M}_k^{(i)}\rangle$, $\mathcal{S}_{kl} = \sum_{i\neq j}\langle \mathcal{M}_k^{(i)}\mathcal{M}_l^{(j)}\rangle$ are the one- and two-body symmetric correlators with $\mathcal{M}_k^{(i)}$ denoting the measurement in direction indexed by $k = \{0, 1\}$ corresponding to particle i. The first inequality equation (17) is particularly fitted to detect non-local correlations in superpositions of Dicke states, while the second inequality equation (18) is tailored to detect non-local correlations in half-filled pure Dicke states [32, 64].

In order to know if there exists a quantum state that violates such Bell inequalities, one still needs to find appropriate n pairs of measurement settings. This gives rise to the so-called Bell operator, a quantum observable in the n-partite Hilbert space whose expectation value with respect to a quantum state corresponds to the value of the Bell inequality for the chosen measurement settings. In general, finding such measurements consist in a very demanding non-convex optimization problem with no trivial solution. However, since the variational ansatz provides a global state, the complexity of the problem gets greatly reduced when we restrict the optimization to the case where all the measurement settings are the same for each party, in the same reference frame. This gives rise to a permutationally invariant Bell operator, whose extremal values within the symmetric space can be found using our VM.

Contrary to previous approaches (see e.g. [32, 65]), where one could use representation theory methods such as Schur–Weyl duality to project the permutationally invariant Bell operator onto the different symmetric blocks (see also [66]), here the VM circumvents this intermediate step: it is enough to consider an effective two-body Bell operator $\tilde{\mathcal{B}}$. For instance, for the Bell inequality in equation (17) the

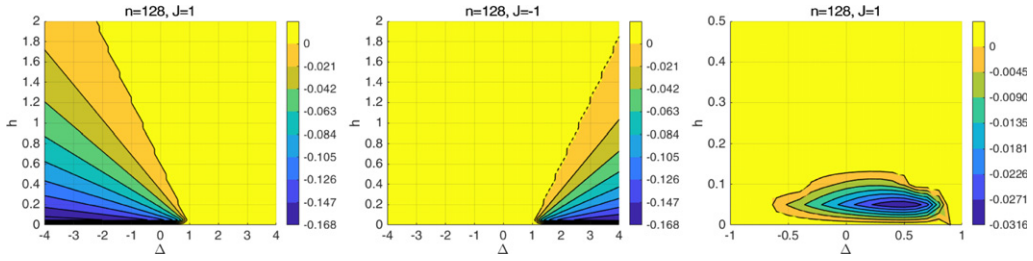

Figure 6. Detection of non-local correlations using inequality equation (17) in the XXZ chain equation (C2) with $n = 128$ particles. Left: Bell inequality value normalized to the classical bound using the VM with equation (19) for $J = 1$ FM couplings. Values below zero indicate non-local correlations with the VM solution. Center: same for $J = -1$ AFM couplings. Right: zoom-in of the region with largest relative violation for the FM case with largest fidelities according to figure 10, conditioned on finding Bell correlations with the VM. Here the expectation values have been computed using the actual ground state given by the DMRG solution with the (non-symmetric) Bell operator equation (21). We have chosen a bond dimension of 32 for the DMRG solution.

corresponding effective Bell operator can be defined as

$$\tilde{\mathcal{B}} := -2n\left(\mathcal{M}_0 \otimes \mathbb{1} + \mathbb{1} \otimes \mathcal{M}_0\right) + \binom{n}{2}\left(\mathcal{M}_0 \otimes \mathcal{M}_0 - 2\mathcal{M}_0 \otimes \mathcal{M}_1 + \mathcal{M}_1 \otimes \mathcal{M}_1\right), \tag{19}$$

so that the Bell inequality in equation (17) reduces to

$$\mathrm{Tr}\left(\tilde{\mathcal{B}}\sigma\right) \geqslant -2n, \tag{20}$$

where σ can be the 2-RDM obtained with the variational ansatz. We parametrize the measurements as $\mathcal{M}_k := \sin(\theta_k)\,\sigma_x + \cos(\theta_k)\,\sigma_z$, where $k \in \{0, 1\}$ and σ_x, σ_z are the Pauli matrices, and use the VM to find the symmetric state minimizing the energy of the effective Hamiltonian. We note that this approach becomes particularly useful in the case of large d, since the number of blocks arising from the symmetry-adapted basis increases with d. We also remark that, since one can always apply a dual $U^{\otimes n}$ symmetry to both state and measurements without departing from the symmetric space, it is enough to optimize over the difference between measurement directions, e.g. $\theta_0 - \theta_1$. Furthermore, since equations (17) and (18) have two inputs and two outputs per party, Jordan's lemma guarantees that using $d = 2$ is sufficient to find its maximal violation.

4.2.2. Looking for Bell non-local correlations in a direction specified by a Hamiltonian

Here we propose a two-step process to find Bell non-local correlations in the ground state of Hamiltonians of physical interest (e.g. an XXZ chain). First, we use the VM to do a quick scan over the parameter space of a given Hamiltonian family, in order to find potential candidates whose ground state might display Bell correlations (see figure 6). If Bell correlations are found by the VM, then a symmetric state has been obtained which displays them, albeit we have no guarantee of the fidelity with the ground state of the model at this point. Second, we narrow down the search to the parameter regime in which nonlocality has been detected and compute the actual ground state with other more computationally expensive methods, such as DMRG (see figure 6).

As toy models we consider an XXZ chain under transverse field (see appendix C.2) and the particular case of a FM XXZ chain with periodic boundary conditions and longitudinal magnetic field (see appendix C.3). As a result, for the first time to the best of our knowledge, we observe that the ground state of the XXZ chain under transverse field in equation (C2) violates the Bell inequality equation (17), thus exhibiting Bell correlations in the corresponding parameter regime. Bear in mind that, in order to carry out the measurement optimization, one can no longer consider a single 2-RDM as we posed in equation (19), but one has to sum over all the different 2-RDMs σ_{ij} obtained with the DMRG. That is, similar to the effective Bell operator approach in equation (19), now the Bell inequality takes the following form:

$$\begin{aligned} -2\sum_{i=1}^{n}\mathrm{Tr}\left(\left(\mathcal{M}_0^{(i)} \otimes \mathbb{1} + \mathbb{1} \otimes \mathcal{M}_0^{(i)}\right)\sigma_i\right) \\ + \sum_{i<j}\mathrm{Tr}\left(\left(\mathcal{M}_0^{(i)} \otimes \mathcal{M}_0^{(j)} - 2\mathcal{M}_0^{(i)} \otimes \mathcal{M}_1^{(j)} + \mathcal{M}_1^{(i)} \otimes \mathcal{M}_1^{(j)}\right)\sigma_{ij}\right) \geqslant -2n. \end{aligned} \tag{21}$$

Also note that, since the RDMs are fixed in this case (by the exact solution), the measurement directions should not be restricted to the XZ plane in the Bloch sphere, but allowed to point in any direction. Furthermore, the measurement settings for each party do not need to coincide.

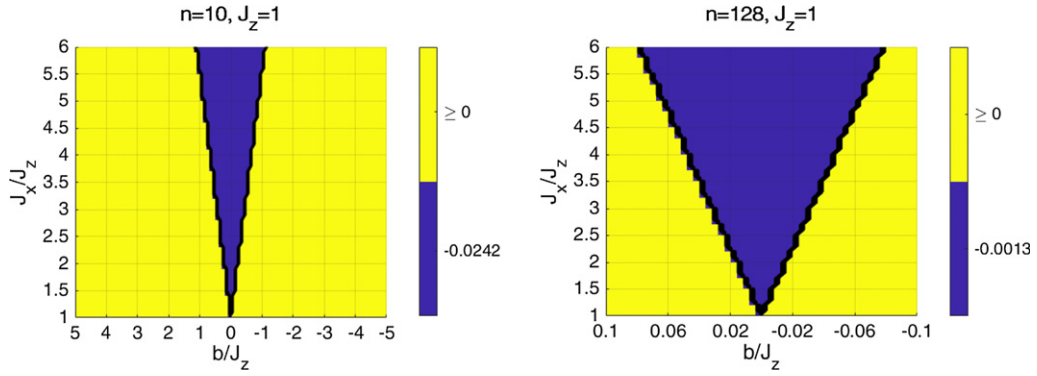

Figure 7. Detection of non-local correlations of the solution given by the VM using inequality equation (18) for the FM XXZ chain with periodic boundary conditions and under a longitudinal magnetic field b equation (C3) with $n = 10$ and $n = 128$ particles respectively. We observe non-local correlations not only in the region where the variational ansatz approximates the ground state with pure half-filled Dicke states, but also where such ansatz approximates the first excited state. Negative numbers indicate the presence of Bell correlations.

We proceed similarly for the FM XXZ chain with periodic boundary conditions and longitudinal magnetic field b presented in appendix C.3, for which pure Dicke states provide a good approximation of the ground state. As we have previously mentioned, inequality equation (18) is tailored to half-filled Dicke states which happen to approximate the ground state in the range $-\frac{1}{n-1}(J_x - J_z) < b < \frac{1}{n-1}(J_x - J_z)$ (see appendix C.3 for details). Therefore, in such region we expect to witness non-local correlations with equation (18). Indeed, in figure 7 we show the witnessed nonlocality, where we have used the variational ansatz to approximate the ground state and optimized using equation (19). We also observe that nonlocality detection goes beyond the specified region where the half-filled Dicke state approximates the ground state. As discussed in appendix C.3, such extra range of nonlocality detection seems to arise from the variational ansatz approximating the first excited state instead of the ground state.

4.3. Generically expressing symmetric states as TI diagonal MPS

In this section we present an analytical method to generically represent any n-qubit Dicke state with a TI MPS. More precisely, the goal is that, given a state of the form

$$|\psi\rangle = \sum_{k=0}^{n} d_k |D_n^k\rangle, \quad d_k \in \mathbb{C}, \tag{22}$$

find two matrices $A_0, A_1 \in \mathcal{M}_{D\times D}(\mathbb{C})$ such that

$$|\psi\rangle = \sum_{(i_1,\ldots,i_n)\in\{0,1\}^n} \psi_{(i_1,\ldots,i_n)} |i_1,\ldots,i_n\rangle = \sum_{(i_1,\ldots,i_n)\in\{0,1\}^n} \mathrm{Tr}[A_{i_1}\ldots A_{i_n}]|i_1,\ldots,i_n\rangle. \tag{23}$$

Some representations of important symmetric states have been known since their inception. For instance, the GHZ state (up to normalization) can be generated with $D = 2$ [67] using the following TI MPS:

$$A_0 = \begin{pmatrix} 1 & 0 \\ 0 & 0 \end{pmatrix}, \qquad A_1 = \begin{pmatrix} 0 & 0 \\ 0 & 1 \end{pmatrix}. \tag{24}$$

On the other hand, for the $|W\rangle$ state, there exists no TI representation with bond dimension 2 [68]. However, it does admit (up to normalization) the following non-TI representation [68]:

$$(A_0^{[i]}, A_1^{[i]}) = \begin{cases} (\sigma^+, \mathbb{1}) & \text{if } i < n \\ (\sigma^+\sigma_x, \sigma_x) & \text{if } i = n. \end{cases} \tag{25}$$

We observe that in equation (25), all the coefficients of the MPS are either 1 or 0. Indeed, some MPS can be used to represent Boolean formula solutions [69]. More generally, the representability of quantum states with MPS of a particular form has deep connections with modern algebraic geometry [70–72]. For instance, the $|W\rangle$ state can be arbitrarily well-approximated with a diagonal TI MPS of bond dimension $D = 2$:

Lemma 1. *Let $\varepsilon > 0$ and*

$$A_0 = \begin{pmatrix} x_0 & 0 \\ 0 & x_1 \end{pmatrix}, \qquad A_1 = \begin{pmatrix} y_0 & 0 \\ 0 & y_1 \end{pmatrix}, \tag{26}$$

where

$$\begin{cases} x_0 = 2^{-1/n}\varepsilon^{-1/[n(n-1)]} \\ x_1 = e^{\mathrm{i}\pi/n}x_0 \\ y_0 = 2^{-1/n}\varepsilon^{1/n} \\ y_1 = -e^{\mathrm{i}\pi/n}y_0. \end{cases} \tag{27}$$

The n-qubit $|W\rangle$ state can be obtained as the limit of $\varepsilon \to 0$ of the TI MPS given by equation (26).

Proof. One simply notes that, since the MPS is diagonal, the element corresponding to the physical index $(i_1, \ldots, i_n)$ with $k := \sum_j i_j$ is given by

$$\psi_{(i_1,\ldots,i_n)} = x_0^{n-k}y_0^k + x_1^{n-k}y_1^k, \tag{28}$$

which amounts to 0 if $k \equiv 0 \bmod 2$ and $\varepsilon^{(k-1)/(n-1)}$ if $k \equiv 1 \bmod 2$. Hence, noting

$$\lim_{\varepsilon\to 0} \varepsilon^{\frac{k-1}{n-1}} = \begin{cases} 1 & \text{if } k = 1 \\ 0 & \text{if } k > 1 \end{cases} \tag{29}$$

yields the result. □

Inspired by lemma 1, we propose now a TI MPS of bond dimension n to approximate *generically* any superposition of Dicke states of the form equation (22). We propose the following parameterization of A_0 and A_1:

$$A_0 \propto \mathbb{1}_D; \qquad A_1 = \mathrm{diag}(x_1, \ldots, x_D). \tag{30}$$

For simplicity let us denote $A_0 = y\mathbb{1}$ and $k = \sum_j i_j$. It is then easy to see that equation (23) leads to the following system of equations:

$$\sum_{a=1}^{D} y^{n-k}x_a^k = \psi_{(i_1,\ldots,i_n)}, \quad \{i_1, \ldots, i_n\} \in \{0, 1\}^n. \tag{31}$$

Note that for states of the form of equation (22) we only require $n + 1$ equations. Hence, it is natural to choose $D = n$. This motivates the following lemma:

Lemma 2. *Consider the system of equations*

$$\begin{cases} x_1 + \cdots + x_n = z_1 \\ x_1^2 + \cdots + x_n^2 = z_2 \\ \quad \cdots \\ x_1^n + \cdots + x_n^n = z_n \end{cases}, \tag{32}$$

where $z_1, \ldots, z_n \in \mathbb{C}$. The solutions of equation (32) are the roots of the polynomial $P(X)$ defined in equation (D10).

Lemma 3. *The system of equations that determines the coefficients y and $x_1 \ldots x_n$ of the diagonal tensors A_0 and A_1, used to represent the linear combination of Dicke states equation (22), is given by*

$$\begin{cases} y & = \sqrt[n]{d_0/n} \\ x_1 + \cdots + x_n & = \dfrac{d_1}{y^{n-1}\sqrt{n}} \\ x_1^2 + \cdots + x_n^2 & = \dfrac{d_2}{y^{n-2}\sqrt{\binom{n}{2}}} \\ \quad \cdots & \\ x_1^k + \cdots + x_n^k & = \dfrac{d_k}{y^{n-k}\sqrt{\binom{n}{k}}} \\ \quad \cdots & \\ x_1^n + \cdots + x_n^n & = d_n \end{cases} \tag{33}$$

The value of y is readily determined from the first equation, and the x's are found by finding the roots of the polynomial $P(X)$ constructed from lemma 2 using the remaining set of equations.

Note that generically, we will have n complex solutions, up to $n!$ permutations. However, there is the possibility that some of the solutions lie at infinity in some pathological cases. Nevertheless, these cases form a zero-measure set which can in practice be avoided by adding an ε-perturbation to d_k, in the same spirit as in equation (27).

It is now clear that the bottleneck is solving equation (32) in lemma 2. We propose two approaches in order to do so: in this section, a variant of the Faddeev–Leverrier algorithm to solve Newton's identities in order to find the roots of power-sum symmetric polynomials. In appendix D, we propose a step-by-step computation of the solutions via Gröbner basis which could provide solutions for more general systems of equations.

We make two observations in order to solve equation (32). The first one is that, if we consider a matrix A with eigenvalues $\{x_1, \ldots, x_n\}$, then equation (32) can be thought of as

$$\mathrm{Tr}[A^k] = z_k, \quad 1 \leqslant k \leqslant n. \tag{34}$$

The second observation is that there exists a way to express the characteristic polynomial of a matrix A in terms of $\mathrm{Tr}[A^k]$. Indeed, if $P(X) = \det(X\mathbb{1} - A) = (X - x_1)\ldots(X - x_n) = \sum_{k=0}^{n} c_k X^k$ is the characteristic polynomial of A, then $P(A) = 0$, and taking the trace in both sides yields such an equation. The Faddeev–Leverrier algorithm provides an easy-to-compute form for the coefficients c_k: they are given by

$$c_{n-m} = \frac{(-1)^m}{m!}\begin{vmatrix} \mathrm{Tr}[A] & m-1 & 0 & \cdots & 0 \\ \mathrm{Tr}[A^2] & \mathrm{Tr}[A] & m-2 & \cdots & \\ \vdots & \vdots & & & \vdots \\ \mathrm{Tr}[A^{m-1}] & \mathrm{Tr}[A^{m-2}] & \cdots & \mathrm{Tr}[A] & 1 \\ \mathrm{Tr}[A^m] & \mathrm{Tr}[A^{m-1}] & \cdots & \cdots & \mathrm{Tr}[A] \end{vmatrix} = \frac{(-1)^m}{m!}\begin{vmatrix} z_1 & m-1 & 0 & \cdots & 0 \\ z_2 & z_1 & m-2 & \cdots & \\ \vdots & \vdots & & & \vdots \\ z_{m-1} & z_{m-2} & \cdots & z_1 & 1 \\ z_m & z_{m-1} & \cdots & \cdots & z_1 \end{vmatrix}. \tag{35}$$

The values of x are found by finding all the roots of the polynomial $P(X) = \sum_{k=0}^{n} c_k X^k$ with $c_n = 1$. In appendix D we give an alternative approach to solve equation (32) from a more algebraic point of view that gives more insight to the combinatorial structure underlying equation (32).

Having an efficient way to represent a state of the form equation (22), we can now use its MPS form to efficiently compute the fidelity of DMRG solutions, which are already given in the MPS formalism, for large n, thus being able to benchmark our method.

4.4. Determining which symmetric states cannot be self-tested from their marginals

Self-testing is one of the most stringent protocols in the paradigm of DI quantum information processing. Self-testing consists in inferring, solely from the statistics of a Bell experiment, which quantum states and measurements are being used and performed, respectively [73–75]. Much of the existing work has been centered around the bipartite case [76, 77], partly motivated by its more accessible physical implementations [78, 79], but also motivated by its more accessible theoretical analysis, exploiting in most cases properties of the maximally entangled state of two qudits [80–82]. In the multipartite case, the analysis becomes more complicated, although some ideas for the bipartite case have inspired some extensions [42]. In the multipartite case, symmetric states constitute a natural candidate to begin their study: for instance, the robust self-testing of the W state ($|D_1\rangle$) [83] inspired schemes to self-test Dicke states of the form $|D_k\rangle$ [42, 43, 84]. Nevertheless, these schemes use full-body correlators and require individual addressing, thus being less appealing from an experimental point of view. Therefore, some studies have been carried to find out whether self-testing is possible using only marginal information [85] (see also [86, 87]): in [85], some efforts showed that the three-qubit states maximally violating some of the translationally invariant, two-body Bell inequalities from [88] could be self-tested using two-body correlators, thus giving a positive answer to this question.

Interestingly, the question of how much information from the statistics is needed (i.e. how many parties one can trace out) in order to self-test a quantum state is still open. In this section, we aim at showing how our method can be used to guarantee a negative answer to the previous question and to give numerical evidence toward a positive answer as well, depending on the uniqueness of the solution to equation (11). More precisely, we show how our method can be used to explore which symmetric states could potentially be self-tested from marginals and which symmetric states definitely could not, because their marginals do not have a unique (modulo local unitaries) extension in the symmetric space.

Let us first consider an n-qubit density matrix being a projector onto an n-qubit Dicke state $|D_k\rangle$ as in equation (1). We shall denote it $\rho_{n,k}$. Let $\sigma = \mathrm{Tr}_1(\rho)$ be the resulting density matrix from tracing out a

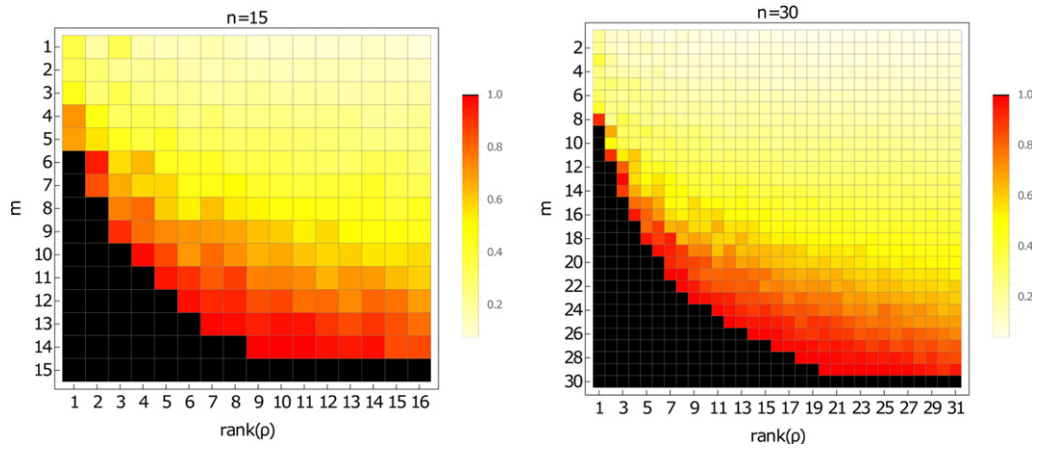

Figure 8. Numerical results on the dependence between n, m, rank(ρ) for an m-RDM to have a unique symmetric extension ρ of $n = 15$ and $n = 30$ qubits respectively with a given rank(ρ). For each case we have carried out 100 trials forcing the SDP to explore the feasible set in a random direction A at each trial. The black squares correspond to the configurations for which the recovered global symmetric state has fidelity > 0.9999 with the original global state for 100% of the trials, thus providing evidence of having a unique symmetric extension. The numerical tolerance has been set to take into account the imprecision of the SDP solver. For the non-black squares, some of the trials have exhibited a fidelity < 0.9999. For those cases, we show the minimal fidelity obtained out of all the trials as a way to illustrate the tolerance. One clearly observes a certain correlation between size of the RDM m and rank(ρ), showing more chances to have a unique extension for low rank(ρ) by tracing out few particles.

single particle. In virtue of equation (7), we have

$$\sigma = \binom{n}{k}^{-1} \left(\binom{n-1}{k-1} \rho_{n-1,k-1} + \binom{n-1}{k} \rho_{n-1,k} \right). \tag{36}$$

To gain some intuition, let us first study under which conditions is it possible to show that the purification of σ is unique. Following the spirit of lemma 5.2 of [89], we begin by considering a purification with an auxiliary system of the form

$$|\Phi\rangle = |D_{k-1}\rangle|P_1\rangle + |D_k\rangle|P_2\rangle, \tag{37}$$

where the Dicke states vectors are supported by the Hilbert space of $n-1$ qubits and

$$|P_1\rangle = \alpha_0|0\rangle|x_{10}\rangle + \alpha_1|1\rangle|x_{11}\rangle \tag{38}$$

$$|P_2\rangle = \beta_0|0\rangle|x_{20}\rangle + \beta_1|1\rangle|x_{21}\rangle, \tag{39}$$

where $|x_{ij}\rangle$ have support in $\mathbb{C}^d$ with a sufficiently large d to represent the purification.

It follows from elementary algebra that the $(n-1)$-body RDM of $|\Phi\rangle\langle\Phi|$ is equal to σ if, and only if,

$$\alpha_0 = 0, \qquad \alpha_1 = \sqrt{\frac{k}{n}}, \qquad \beta_0 = \sqrt{\frac{n-k}{n}}, \qquad \beta_1 = 0. \tag{40}$$

Hence, in this case there exists a purification, it is unique, and it must be of the form

$$|\Phi\rangle = |D_N^k\rangle|x_{11}\rangle. \tag{41}$$

Corollary 1. *The $(n-1)-$partite reduced state of $|D_k\rangle$ uniquely determines $|D_k\rangle$ in the symmetric space.*

In appendix E we show how the above example can be generalized to tracing out any number of parties. The uniqueness of the extension is in one-to-one correspondence to the uniqueness of a linear program (see equation (E9)). We have numerically observed that such a solution is unique if we trace out up to $n-2$ parties for a basis Dicke state. However, it is not *a priori* clear how generic the above property is. A more in-depth study suggests that generically, the uniqueness property depends on both the rank of the global density matrix and the number of parties traced out. In figure 8 we provide numerical evidence that generically the uniqueness of the symmetric extension depends on the number of particles n, the number m of parties in the RDMs and the rank of the global density matrix ρ. We have followed the procedure below:

(a) Generate a random symmetric state whose density matrix has a given rank
(b) Use the compatibility conditions to obtain its RDM

(c) Choose a random Hermitian matrix A and find a new global state compatible with the RDM by making use of the SDP in equation (11), but with objective function $-\langle A, \rho\rangle$ and check its fidelity with the original global state. The matrix A forces the SDP to explore the feasible set in the direction given by A

(d) We repeat step (c) a sufficient number of times (in our case, 100 times). If the fidelity remains always one up to numerical accuracy error, this is strong numerical evidence that the global state is unique. On the other hand, if the fidelity falls below one in some case, this indicates that too many parties have been traced out and the RDM would no longer be sufficient to self-test the original state, since it does not have a unique global extension of size n

We note that, although mixed states in their generality cannot be self-tested, the fact that for some rank configurations and sizes of the RDM the extension to the symmetric state seems to be unique could open the door to a weaker form of self-testing, under the assumption that the global state is symmetric.

5. Conclusions and outlook

In the present work we have presented a study of the QMP restricted to symmetric states. We have provided a complete set of analytical compatibility conditions for an m-qudit RDM σ to be compatible with an n-qudit global symmetric state ρ. We then use said compatibility conditions to answer the question of whether a given reduced density matrix σ is compatible with a global symmetric state ρ by turning it into a feasibility problem efficiently solvable via an SDP. Our results have implications in different fields. We have explored some of them in several case-studies:

- We have developed a computationally efficient variational optimization method to upper bound the ground state energy of any local Hamiltonian. This method considers the resulting marginals to be compatible with a global symmetric state in order to carry out the optimization by means of SDP with the compatibility conditions as constraints. In order to benchmark the VM, we have considered several paradigmatic Hamiltonian spin models, that go from long-range to nearest-neighbor interactions. In general, we observe that the VM provides a good upper bound for FM and long-range interactions, yielding exact results in the infinite-range limit; while it misses to capture AFM short-range interactions, where the ground state has poor overlap with the symmetric space. We have also used the compatibility conditions in order to obtain the half-system entanglement entropy in the symmetric space, which is an insightful quantity for many-body systems. Remarkably, we present numerical evidence that for some cases our VM can also be used to approximately locate phase transitions. This numerical observation hints that the properties of the ground state in a phase transition also manifest, to some extent, in the symmetric space projection and are, therefore, captured by our method. Another observed feature is that for some specific models the VM has recovered the first excited state, instead of the ground state, in some regions of the phase diagram. Finally, we have observed a significant speed advantage of the VM compared to a typical DMRG algorithm. The advantage of the VM lies on the low memory storage required and high speed, making the VM a suitable candidate for a first order exploration of large sets of parameters characterizing the phase diagram of spin Hamiltonians. While we have only considered qubits, qutrits and chain configurations, our VM is straightforwardly applicable to any qudit and lattices of arbitrary geometry and dimension. We leave open to implement and explore the VM in corresponding cases of interest.
- We have considered the VM in the context of Bell non-local correlations. In particular, we have explored its synergy with the so-called two-body permutationally invariant Bell inequalities. The results in this context are two-fold: first, we have shown how the VM comes as a natural tool to optimize a multipartite two-body PIBI in order to find whether the inequality detects non-local correlations; second, we have used the low computational cost of the VM to look for non-local correlations in a spin-1/2 XXZ chain under a transverse field, narrowing the parameters to be considered and eventually leading to the detection of non-local correlations in the ground state with $n = 128$ parties. We have also considered another spin-1/2 XXZ chain this time with periodic boundary conditions with longitudinal magnetic field, detecting non-local correlations on its ground state and first excited state of a specific phase. The tool we have here presented can be readily used in the context of Bell correlation depth [90] or DI entanglement depth certification [91, 92] in the context of two-body PIBIs.
- We have developed an analytical methodology to derive a translationally invariant diagonal matrix-product state representation of bond dimension n for pure symmetric states. This result is generic, and could be of independent interest. For our purposes, we have used it to transform the

symmetric state solution obtained with the VM into a translationally invariant, diagonal, MPS, allowing us to check its fidelity with the DMRG solution.

- Finally, we have shown how the compatibility conditions can be used to determine which symmetric states ρ cannot be self-tested solely from their marginals. Remarkably, we present numerical evidence suggesting a correlation between the size of the global state n, its rank $\mathrm{rank}(\rho)$, how many particles m remain in the observed RDM and the uniqueness of a symmetric global state. This uniqueness property could open the way to a weaker form of self-testing, that uses the assumption that the global state is symmetric.

Our work, however, is not limited to the above applications. For instance, on a recent work by us we have used the present work to tackle the problem of bounding the fidelity of a many-body quantum state in atomic ensembles [93]. Further interesting connections that deserve to be explored include symmetric extensions of quantum states, intimately related to the separability problem, which are also naturally treated as SDP [23, 94], with direct applications to symmetric and permutationally invariant states [95, 96]. Furthermore, one may also wish to explore the role of different symmetries in the SDP. Whether there exists a SDP invariant formulation of our problem [66, 97] that could allow it to be formulated for other symmetry groups is unclear and we leave it for future research. In a following work, we shall investigate variations of the VM in order to perform tomography/fidelity estimates with respect to a target symmetric state. This is of wide experimental relevance, as in the case of Bose–Einstein condensate where only partial information (e.g. not an informationally complete set of measurements) is available [31, 98].

Acknowledgments

We thank A Acín, F Huber and M Sanz for inspiring discussions. MF acknowledges support from the Swiss National Science Foundation. JT thanks the Alexander von Humboldt foundation for support. This project has been funded by the European Union's Horizon 2020 research and innovation programme under Grant Agreement No. 899354 and the Deutsche Forschungsgemeinschaft (DFG, German Research Foundation)—Project No. 414325145 in the framework of the Austrian Science Fund (FWF): SFB F71. AA acknowledges support received from ERC AdG NOQIA, Spanish Ministry MINECO and State Research Agency AEI (FIDEUA PID2019-106901GB-I00/10.13039/501100011033, SEVERO OCHOA No. SEV-2015-0522 and CEX2019-000910-S, FPI), European Social Fund, Fundació Cellex, Fundació Mir-Puig, Generalitat de Catalunya (AGAUR Grant No. 2017 SGR 1341, CERCA program, QuantumCAT U16-011424, co-funded by ERDF Operational Program of Catalonia 2014–2020), MINECO-EU QUANTERA MAQS (funded by State Research Agency (AEI) PCI2019-111828-2/10.13039/501100011033), EU Horizon 2020 FET-OPEN OPTOLogic (Grant No. 899794), and the National Science Center, Poland-Symfonia Grant No. 2016/20/W/ST4/00314.

Data availability statement

The data that support the findings of this study are available upon reasonable request from the authors.

Appendix A. Proof of theorem 1

We begin by noting that, in the computational basis, the partial trace of $n-m$ subsystems of an n-qudit density matrix ρ has the following expression:

$$\mathrm{Tr}_{n-m}(\rho) = \sum_{\vec{i},\vec{j}\in[d]^m} |\vec{i}\rangle\langle\vec{j}| \sum_{\vec{k}\in[d]^{n-m}} \rho_{\vec{j}|\vec{k}}^{\vec{i}|\vec{k}}, \tag{A1}$$

where the operator $|$ denotes index concatenation, and the indices have been properly rearranged so that the $n-m$ traced out parties are the last ones.

Hence, our goal is to express the symmetric state in the computational basis in order to apply equation (A1) and then go back to the symmetric space. Since Dicke states are enumerated by the partitions of m it will be useful to define the following function:

$$\begin{array}{rccc} w_k\colon & [d]^n & \longrightarrow & \{0,\ldots,n\} \\ & \vec{i} & \mapsto & \#\{p\in[n] : i_p = k\} \end{array} \tag{A2}$$

In words, $w_k(\vec{i})$ counts how many coordinates of $\vec{i}$ are equal to k. It is then natural to define $\boldsymbol{w}(\vec{i}) := (w_0(\vec{i}),\ldots,w_{d-1}(\vec{i}))$. Note that, by construction, $\boldsymbol{w}(\vec{i}) \vdash n$ for every $\vec{i}\in[d]^n$.

The weight counting function $\boldsymbol{w}$ is useful to represent the Dicke state $|\boldsymbol{\lambda}\rangle$ in the computational basis. For the purpose of this proof, we use the notation $|D_{\boldsymbol{\lambda}}\rangle$ to specify that the Dicke state is in the computational basis representation:

$$|D_{\boldsymbol{\lambda}}\rangle = \binom{n}{\boldsymbol{\lambda}}^{-1/2} \sum_{\vec{i}\in[d]^n} |\vec{i}\rangle \delta(\boldsymbol{w}(\vec{i}) - \boldsymbol{\lambda}), \tag{A3}$$

where δ is the Kronecker Delta function, which is 1 if, and only if, its argument is the zero vector; 0 otherwise. Thanks to equation (A3) we can now define the inclusion operator $\Pi : \mathrm{Sym}(\mathbb{C}^d)^{\otimes n} \hookrightarrow (\mathbb{C}^d)^{\otimes n}$ onto the symmetric space

$$\Pi := \sum_{\boldsymbol{\lambda}\vdash n} |D_{\boldsymbol{\lambda}}\rangle\langle\boldsymbol{\lambda}|. \tag{A4}$$

We note that $\Pi^\dagger\Pi = \mathbb{1}_{\mathrm{Sym}(\mathbb{C}^d)^{\otimes n}}$ and that $\Pi^\dagger : (\mathbb{C}^d)^{\otimes n} \twoheadrightarrow \mathrm{Sym}(\mathbb{C}^d)^{\otimes n}$ is the projector onto the symmetric space.

Let now ρ be a density matrix on $\mathrm{Sym}(\mathbb{C}^d)$, whose components are labeled $\rho^{\boldsymbol{\lambda}}_{\boldsymbol{\mu}}$ in the Dicke basis and $\rho^{\vec{i}}_{\vec{j}}$ in the computational basis. The relation between them is given by

$$\rho^{\vec{i}}_{\vec{j}} = \left(\Pi(\rho^{\boldsymbol{\lambda}}_{\boldsymbol{\mu}})\Pi^\dagger\right)^{\vec{i}}_{\vec{j}} = \sum_{\tilde{\boldsymbol{\lambda}},\tilde{\boldsymbol{\mu}}\vdash n} \delta(\boldsymbol{w}(\vec{i}) - \tilde{\boldsymbol{\lambda}})\delta(\boldsymbol{w}(\vec{j}) - \tilde{\boldsymbol{\mu}}) \binom{n}{\tilde{\boldsymbol{\lambda}}}^{-1/2} \binom{n}{\tilde{\boldsymbol{\mu}}}^{-1/2} \rho^{\tilde{\boldsymbol{\lambda}}}_{\tilde{\boldsymbol{\mu}}}. \tag{A5}$$

Now we are ready to trace out $n - m$ parties of ρ, e.g. the last. Note that $\boldsymbol{w}(\vec{a}|\vec{b}) = \boldsymbol{w}(\vec{a}) + \boldsymbol{w}(\vec{b})$. Hence, using equation (A1) we obtain $\sigma := \mathrm{Tr}_{n-m}(\rho)$ as

$$\sigma^{\vec{i}}_{\vec{j}} = \sum_{\vec{k}\in[d]^{n-m}} \rho^{\vec{i}|\vec{k}}_{\vec{j}|\vec{k}} = \sum_{\boldsymbol{\lambda},\boldsymbol{\mu}\vdash n} \rho^{\boldsymbol{\lambda}}_{\boldsymbol{\mu}} \binom{n}{\boldsymbol{\lambda}}^{-1/2} \binom{n}{\boldsymbol{\mu}}^{-1/2} \sum_{\vec{k}\in[d]^{n-m}} \delta(\boldsymbol{w}(\vec{i}) + \boldsymbol{w}(\vec{k}) - \boldsymbol{\lambda})\delta(\boldsymbol{w}(\vec{j}) + \boldsymbol{w}(\vec{k}) - \boldsymbol{\mu}), \tag{A6}$$

yielding equation (7). Finally, equation (8) is obtained via the transformation $(\sigma^{\boldsymbol{\alpha}}_{\boldsymbol{\beta}}) = \Pi^\dagger(\sigma^{\vec{i}}_{\vec{j}})\Pi$. □

Appendix B. Basics of semidefinite programming

Semidefinite programming (SDP) is a class of convex, constrained optimization problems which constitutes one of the main theoretical and computational techniques in convex algebraic geometry [45]. In particular, SDP takes Hermitian matrices as optimization variables and optimizes linear functions subject to linear matrix inequalities (LMIs). The set of matrices that satisfy all the LMIs in the problem constitutes the so-called feasible region (which may be empty if no matrix satisfies all the LMIs simultaneously). In mathematical terms, the feasible region of an SDP problem is called a *spectrahedron*, and it is then the intersection between some affine linear subspace (given by the LMIs) and the cone of positive symmetric matrices. Note that the feasible region will always be convex since it is the intersection of convex sets.

Such conditions grant SDP problems desirable numerical properties, which allow for efficient solutions by numerical algorithms based on, e.g. the interior point methods and the primal-dual method. Moreover, the optimality of the solution given by said algorithms is by construction a certificate or, in other words, a numerical mathematical proof. Consequently, SDP has found success in many distinct fields. For instance, the interest of using SDP in quantum information problems keeps increasing and is crucial for topics like non-local correlations [64, 99], quantum steering [100] or separability [94].

The general **primal** SDP formulation can be stated as follows:

$$\begin{aligned} &\min_X \ \langle C, X\rangle \\ &\text{s.t. } X \succeq 0 \\ &\langle A_i, X\rangle = b_i \quad i = 1, \ldots, m, \end{aligned} \tag{B1}$$

where $\langle X, Y\rangle = \mathrm{Tr}(X^\dagger Y)$ is the Hilbert–Schmidt scalar product, C, A_i, X are $n \times n$ Hermitian matrices, and X is the matrix variable over which the optimization is performed. Notice that in the cases presented in the main text, we treat X as a density matrix (thus we require it to be positive semidefinite and have unit trace).

If there exists a set of matrices which satisfies the given constraints forming a spectrahedron (i.e. the feasible set), then the SDP problem is said to be *feasible* and has at least one solution. Conversely, the SDP problem is said to be *infeasible* when the spectrahedron cannot be formed by the given constraints. Therefore, the SDP formulation in (B1) can be turned into a *feasibility problem* by taking the objective function to be a constant independent of the decision variables (i.e. by making the objective function

irrelevant) and using the algorithms to probe only for the non-emptiness of the spectrahedron. For instance, one way to pose (B1) as a feasibility problem is to consider the particular case where $C = 0_{n,n}$ is the $n \times n$ zero matrix and, therefore, $\langle C, X\rangle = 0$.

An important feature of SDP problems is that to every primal SDP formulation there exists an associated **dual** SDP problem which is stated as follows:

$$\begin{aligned} &\max_{y} \; b^T y \\ &\text{s.t.} \sum_{i=1}^{m} A_i y_i \preceq C, \end{aligned} \tag{B2}$$

where $b = (b_1, \ldots, b_m)$ and $y = (y_1, \ldots, y_m)$ are the dual decision variables. The relevance of having a dual formulation comes clear by noting that, by construction, the dual optimal value provides an upper bound on the primal optimal value. In particular, it can be easily checked that the difference between any primal and dual feasible solutions X and y is:

$$\langle C, X\rangle - b^T y = \langle C - \sum_{i=1}^{m} A_i y_i, X\rangle \geqslant 0, \tag{B3}$$

which is known as the *duality gap*, and the inequality $\langle C, X\rangle \geqslant b^T y$ for any feasible matrix X and vector y is known as the *weak duality*. Therefore, by evaluating the objective function of (B1) with any feasible matrix X, one obtains an upper bound on the objective function of (B2) (and viceversa to obtain a lower bound on the objective function of (B1)). Moreover, when considering a feasibility problem and obtaining an infeasible solution, the dual problem can be used to certify the non-existence of solutions in the primal problem. In most non-pathological cases (e.g. when strict feasibility is present [45]) the duality gap is closed for an optimal pair (X^*, y^*), yielding strong duality and a certificate of convergence.

Appendix C. Variational method: further examples

C.1. Ising chain for nearest neighbors interactions

In section 4.1.2 we explored how our VM behaves as we decrease the range of interactions on an Ising chain with power-law decaying interactions, and in section 4.1.1 we focused on the extreme case of having infinite-range interactions (the LMG). Here we investigate what happens in the other extreme case: an Ising model with nearest-neighbours interactions in a transverse field. The Hamiltonian we consider is:

$$\mathcal{H} = -J_z \sum_{i=1}^{n-1} \sigma_z^{(i)} \sigma_z^{(i+1)} - h \sum_{i=1}^{n} \sigma_x^{(i)}, \tag{C1}$$

where $J_z > 0$ ($J_z < 0$) corresponds to FM (AFM) coupling, and h tunes the transverse field strength. For equation (C1), the VM is taken with the effective Hamiltonian $\tilde{\mathcal{H}} := -(n-1)J_z \sigma_z \otimes \sigma_z - nh(\sigma_x \otimes \mathbb{1} + \mathbb{1} \otimes \sigma_x)/2$. Similar as done in sections 4.1.1 and 4.1.2, in figure 9 we compare the VM with ED for low number of particles. As expected, the VM yields almost orthogonal solutions in the AFM region, while it provides fidelities close to unity in the FM region. Still, slight discrepancies arise in the FM case. In particular, one observes that in the vicinity of what is a critical point (in the asymptotic limit) the fidelity drops, nevertheless still providing a good upper bound to the ground state energy (see figure 9). We remark that, by using the VM to determine the half-system entropy scaling in the FM case ($J_z = 1/2$), we observe an anomaly at $h \approx 1$ (see figure 9), which signals the presence of critical point. Therefore, despite the discrepancy in fidelity, the FM critical point can still be well approximated by our VM.

C.2. XXZ model under a transverse field

In appendix C.1 we have looked at a spin system in one dimension and with nearest-neighbour interactions. This model is actually solvable via Jordan–Wigner transformation [101], as it can be equivalently described as a system of free fermions (see e.g. [46]). Here we consider the validity of our variational ansatz beyond the free fermion scope, in an XXZ spin chain with an homogeneous magnetic field in the X direction:

$$\mathcal{H} = -J \sum_{\langle i,j\rangle} \left(\sigma_x^{(i)} \sigma_x^{(j)} + \sigma_y^{(i)} \sigma_y^{(j)} + \Delta \sigma_z^{(i)} \sigma_z^{(j)}\right) + \sum_i h \sigma_x^{(i)}, \tag{C2}$$

where we take $J = 1$ ($J = -1$) for the FM (AFM) couplings, Δ marks the anisotropy (with $\Delta = 1$ corresponding to the isotropic case, the XXX model) and h tunes the transverse field strength. In this case,

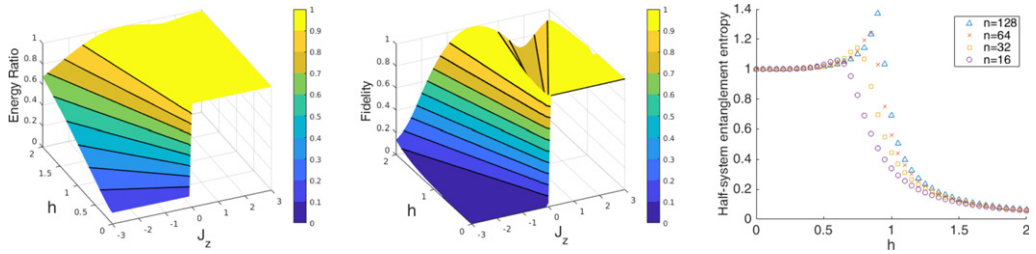

Figure 9. Numerical results for the Ising Hamiltonian (C1) with $n = 10$. Left and center: comparison of the ground state energy and fidelity with respect to results from exact diagonalization. We observe that energies disagree mostly in the AFM case, due to its inherent asymmetry. The FM case is in general well approximated, with only some minor discrepancies near the values that hint at a critical point in the asymptotic limit. Right: the VM is used in the FM case ($J_z = 1/2$) in order to investigate the scaling of the half-system entanglement entropy, hinting at the existence of a critical point when extrapolating to the asymptotic limit.

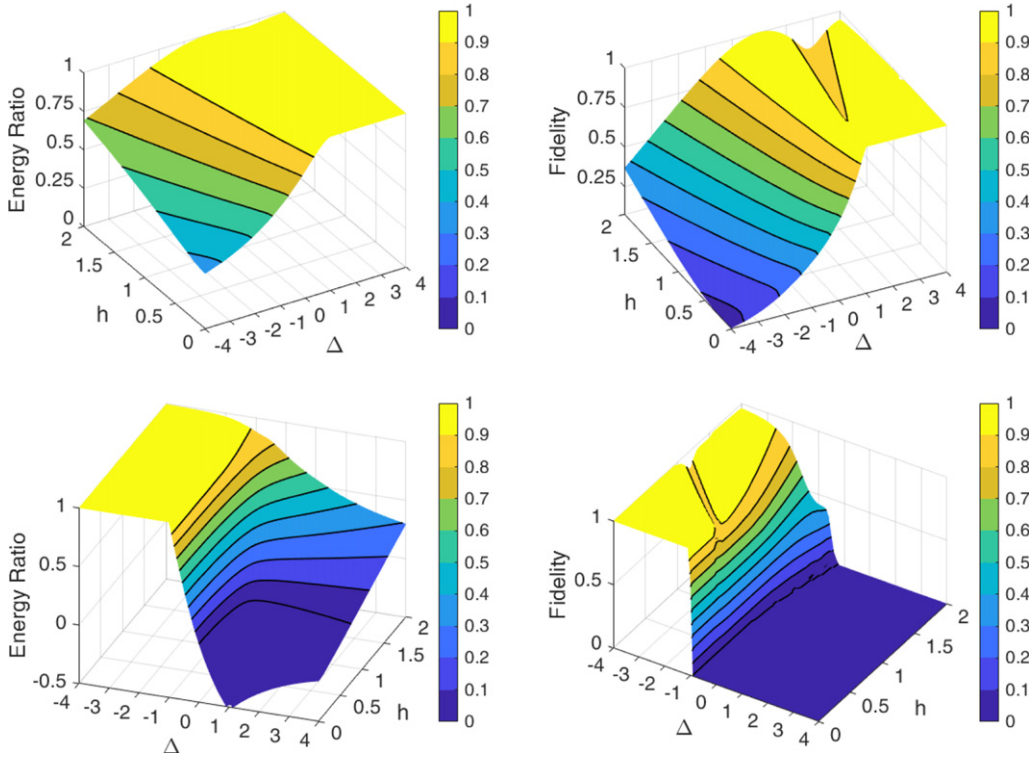

Figure 10. Numerical results for the XXZ Hamiltonian (C2) with $n = 10$, compared to exact diagonalization. The first row corresponds to FM interactions ($J = 1$) while the second row corresponds to AFM interactions ($J = -1$). Left: ground energy ratio. Right: ground state fidelity. We observe how the ground state fidelity and energy are well approximated for values $\Delta \gtrsim 1$ ($\Delta \lesssim -1$) when considering FM (AFM) interactions. In such regime it provides close to exact results except in the vicinity of the phase transition between regions 2–3 and 2–4 of figure 1 of [102].

the effective Hamiltonian for the VM is $\tilde{\mathcal{H}} := J\left((n-1)\left(\sigma_x \otimes \sigma_x + \sigma_y \otimes \sigma_y + \Delta\sigma_z \otimes \sigma_z\right) + nh(\sigma_x \otimes \mathbb{1} + \mathbb{1} \otimes \sigma_x)/2\right)$.

In figure 10 we compare the ground states obtained from our VM with those obtained from ED, in terms of relative energy and fidelity. For this case we observe numerically that the VM provides a faithful approximation for values $\Delta \gtrsim 1$ ($\Delta \lesssim -1$) when considering FM (AFM) interactions. In particular, in such a regime the VM yields exact results except around a line which likely corresponds to critical points in the asymptotic limit [102, 103].

C.3. Ferromagnetic XXZ with periodic boundary conditions

Let us now consider the following instance of an XXZ model: a periodic anisotropic FM spin-1/2 chain, placed in an homogeneous magnetic field in the z direction. This model is described by the Hamiltonian

$$\mathcal{H} = -J_x \sum_{i=1}^{n} \left(\sigma_x^{(i)} \otimes \sigma_x^{(i+1)} + \sigma_y^{(i)} \otimes \sigma_y^{(i+1)}\right) - J_z \sum_{i=1}^{n} \sigma_z^{(i)} \otimes \sigma_z^{(i+1)} + b \sum_{i=1}^{n} \sigma_z^{(i)}, \tag{C3}$$

Table 1. Ground state for the model in equation (C3), as a function of the magnetic field b and the coupling parameter $\Delta J = J_x - J_z$, according to the perturbative results presented in [104]. In figure 11 we recover and strengthen the result.

b	Ground state
$b < -\Delta J$	$\vert D_0^n\rangle$
$-\frac{n-2k+1}{n-1}\Delta J < b < -\frac{n-2k-1}{n-1}\Delta J$	$\vert D_k^n\rangle, 0 < k < n$
$\Delta J < b$	$\vert D_n^n\rangle$

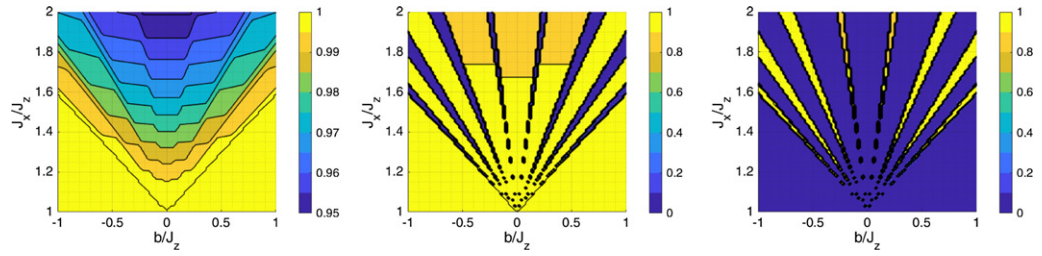

Figure 11. Numerical results for the XXZ model equation (C3) with $n = 10$, compared to exact diagonalization. Left: energy ratios. Center: ground state fidelity. Right: first excited state fidelity. We note that the overlap of the right and center figures would cover the whole phase diagram.

where $\sigma^{(n+1)} = \sigma^{(1)}$, $J_x, J_z \geqslant 0$ are the exchange coupling constants, and b tunes the strength of the external magnetic field. The preparation of Dicke states as ground states of equation (C3) has been studied in reference [104], for which our variational ansatz comes as a natural tool to benchmark their fidelity. In table 1 we show the ground state distribution predicted with the perturbative results of [104] and in figure 11 we see that, up to $n = 10$, the fidelity remains $> 85\%$, which is consistent with the predictions of [104]. For this case, in the VM we take the effective Hamiltonian $\tilde{\mathcal{H}} := -n\left(J_x\left(\sigma_x \otimes \sigma_x + \sigma_y \otimes \sigma_y\right)\right.$ $\left. + J_z\sigma_z \otimes \sigma_z\right) + nb(\sigma_z \otimes \mathbb{1} + \mathbb{1} \otimes \sigma_z)/2$.

The perturbative prediction from [104] splits the phase diagram among different regions, each having substantial overlap to a different Dicke state. However, there are already some discrepancies observed: in between these regions, the approximation with Dicke states does not have good overlap with the ground state (see figure 1 in [104]), however it has good overlap with other basis Dicke states (see figure 2 in [104]). Here, our method enables us to understand this discrepancy from a different perspective: in figure 11 we see that the regions in which the perturbative approach fails actually correspond to a good overlap for the first excited state and a Dicke state. The low-end of the spectrum of the Hamiltonian considered has a good overlap with the symmetric space. However, it can happen that the VM chooses to approximate the first excited state instead of the ground state if the energy obtained becomes more favorable. This depends on both the overlap with the ground space and the energy gap of the Hamiltonian. Let us denote by E_0 and by E_1 the ground and first excited state energies, respectively. Let us also denote by F_0 (F_1) the fidelity between the ground state (first excited state) and the symmetric space. The discontinuities may happen when $F_0E_0 = F_1E_1$. Indeed, in figure 11 we observe that, while the energy ratio is smooth, the fidelity may suddenly drop to zero or jump to almost one due to the above mentioned reason.

For the larger n limit, the ground state of equation (C3) can be found exactly using MPS and the DMRG algorithm, case for which the representation of superpositions of Dicke states as an MPS presented in section 4.3 might come in handy.

C.4. Many-body $SU(3)$ Hamiltonian with collective interactions

Here we illustrate that our proposed VM can be also easily applied to d-level systems with local Hilbert space of dimension $d > 2$. To do so, we consider the three-orbital LMG Hamiltonian [105] (equivalently, the generalisation of the Lipkin Hamiltonian as proposed in [25]). Similarly to section 4.1.1, the variational ansatz is expected to recover exact results due to the long-range interactions resulting in ground states with permutation symmetry. The model is constructed by n identical but distinguishable three-level atoms, and it is also commonly used in nuclear shell models. It can also arise for three-level atoms collectively coupled to electromagnetic field modes of a cavity. Concretely, the model is described by the Hamiltonian:

$$\mathcal{H} = a\left(\mathcal{S}_{00} - \mathcal{S}_{22}\right) + b\sum_{i\neq j}\mathcal{S}_{ij}^2, \tag{C4}$$

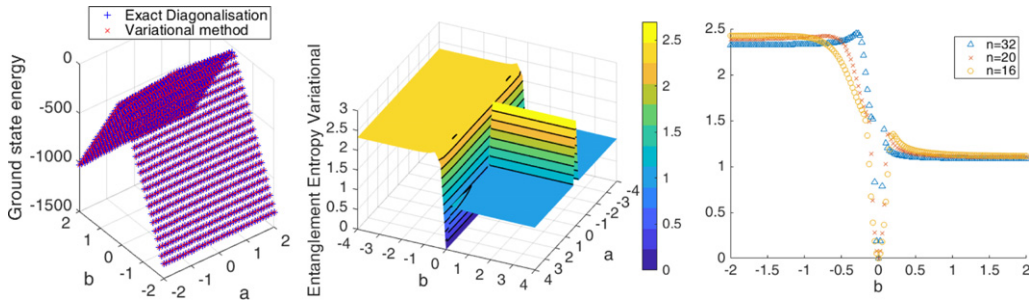

Figure 12. Numerical results for the three-level generalized Lipkin Hamiltonian equation (C4) with $n = 32$. Left: the VM provides exact ground state up to numerical error of the solver ($\approx 10^{-14}$ using SeDuMi [54]). Center: half-system entanglement entropy obtained through the compatibility conditions equation (8), capturing features of phase transitions. Right: half-system entanglement entropies for different number of particles at $a = 3$. The scalability can be used to extrapolate the peak anomalies to the asymptotic limit.

where $\mathcal{S}_{ij} = \sum_{l=1}^{n} \tau_{ij}^{(l)}$ with $\tau_{ij} = |i\rangle\langle j|$ for $i, j = \{0, 1, 2\}$. In this case the effective Hamiltonian used in the SDP is $\tilde{\mathcal{H}} := na\left(\mathcal{S}_{00} \otimes \mathbb{1} + \mathbb{1} \otimes \mathcal{S}_{00} - \mathcal{S}_{22} \otimes \mathbb{1} - \mathbb{1} \otimes \mathcal{S}_{22}\right)/2 + \binom{n}{2} b \sum_{i \neq j} \left(\mathcal{S}_{ij} \otimes \mathcal{S}_{ij} + (\mathcal{S}_{ij}^2 \otimes \mathbb{1} + \mathbb{1} \otimes \mathcal{S}_{ij}^2)/2\right)$.

In figure 12 we show that the variational ansatz reproduces exactly the ground state energy, as expected. Furthermore, we use the compatibility conditions to obtain the half-system entanglement entropy, which is useful to provide insights about the phase diagram of the model.

Appendix D. Alternative solution to the system of equations in lemma 2

Before introducing the form of $P(X)$ let us motivate its definition by illustrating the idea with a sequence of examples. In these examples, we turn equation (32) into an equivalent system that is much easier to solve. In algebraic geometry terms, the second system forms a reduced Groebner basis, meaning that its first equation is a polynomial in a single variable, the second is a polynomial in the previous variable and a new one, etc. This allows one to find all the solutions by solving only univariate polynomials and plugging the found roots into the next equations by substitution.

- $N = 2$. Solving the system of equations

$$\begin{cases} x_1 + x_2 - z_1 = 0 \\ x_1^2 + x_2^2 - z_2 = 0 \end{cases} \tag{D1}$$

is equivalent to solving

$$\begin{cases} 2x_2^2 - 2z_1 x_2 + (z_1^2 - z_2) = 0 \\ x_1 + x_2 - z_1 = 0 \end{cases} \tag{D2}$$

- $N = 3$. Solving the system of equations

$$\begin{cases} x_1 + x_2 + x_3 - z_1 = 0 \\ x_1^2 + x_2^2 + x_3^2 - z_2 = 0 \\ x_1^3 + x_2^3 + x_3^3 - z_3 = 0 \end{cases} \tag{D3}$$

is equivalent to solving

$$\begin{cases} 6x_3^3 - 6z_1 x_3^2 + 3(z_1^2 - z_2)x_3 + (-z_1^3 + 3z_1 z_2 - 2z_3) = 0 \\ 2x_3^2 - 2(z_1 - x_2)x_3 + [(z_1 - x_2)^2 - (z_2 - x_2^2)] = 0 \\ x_2 + x_3 - (z_1 - x_1) = 0 \end{cases} \tag{D4}$$

- $N = 4$. Solving the system of equations

$$\begin{cases} x_1 + x_2 + x_3 + x_4 - z_1 = 0 \\ x_1^2 + x_2^2 + x_3^2 + x_4^2 - z_2 = 0 \\ x_1^3 + x_2^3 + x_3^3 + x_4^3 - z_3 = 0 \\ x_1^4 + x_2^4 + x_3^4 + x_4^4 - z_4 = 0 \end{cases} \tag{D5}$$

is equivalent to solving

$$\begin{cases} 24x_4^4 - 24z_1x_4^3 + 6(z_1^2 - z_2)x_4^2 - 2(z_1^3 - 3z_1z_2 + 2z_3)x_4 + (z_1^4 - 6z_1^2z_2 + 3z_2^2 + 8z_1z_3 - 6z_4) = 0 \\ 6x_4^3 - 6(z_1 - x_3)x_4^2 + 3([z_1 - x_3]^2 - [z_2 - x_3^2])x_4 - ([z_1 - x_3]^3 - 3[z_1 - x_3][z_2 - x_3^2] + 2[z_3 - x_3^3]) = 0 \\ 2x_4^2 - 2(z_1 - x_2 - x_3)x_4 + [(z_1 - x_2 - x_3)^2 - (z_2 - x_2^2 - x_3^2)] = 0 \\ x_2 + x_3 + x_4 - (z_1 - x_1) = 0 \end{cases} \tag{D6}$$

From the above examples the recursion is clear. In the *easy* systems equations (D2), (D4), (D6) the first equation is a polynomial in a single variable x_n. The rest of the equations correspond to the system of equations for $n-1$ with a slight transformation, where we have decreased by 1 the index of x_i; i.e. $x_i \mapsto x_{i-1}$ and we have made the substitution $z_i \mapsto z_i - x_{n-1}^i$ in the first equation, $z_i \mapsto z_i - x_{n-2}^i$ in the second equation and so on until we substitute $z_1 \mapsto z_1 - x_1$ in the last one. Note that since the first equation is a polynomial in x_n, the second equation is a polynomial in x_n, x_{n-1}, the third equation a polynomial in x_n, x_{n-1}, x_{n-2} and so on the transformed systems form a reduced Groebner basis and are therefore easy to solve.

Before thinking of writing the Groebner basis in its full generality, let us observe the following:

Corollary 2. *Let $P(X)$ be the first element of the Groebner basis for equation (32) (i.e. the left-hand side of the first equation in the systems equations (D2), (D4), (D6), etc). Since the system of equations (32) is permutationally invariant, we must have*

$$P(X) = (X - x_1)\dots(X - x_n), \tag{D7}$$

i.e. the roots of P correspond to the values of x_i, up to a permutation.

Therefore, we only need to find the general form of $P(X)$. The coefficients of $P(X)$ are closely related to the partitions of n. Let us define the following:

Definition 1. Let $\boldsymbol{\lambda} \vdash m$ denote a partition of m; i.e. $\boldsymbol{\lambda} = (\lambda_1^{\mu_1}, \dots \lambda_k^{\mu_k})$ where $\sum_{i=1}^k \mu_i\lambda_i = m$ and $\lambda_i > \lambda_{i+1}$ with $\lambda_i, \mu_i \in \mathbb{N}$. We define the polynomial

$$Q_m(\boldsymbol{z}) := \sum_{\boldsymbol{\lambda}\vdash m} \xi_{\boldsymbol{\lambda}} \prod_{i=1}^{k} z_{\lambda_i}^{\mu_i}, \tag{D8}$$

where

$$\xi_{\boldsymbol{\lambda}} = m! \prod_{i=1}^{k} \frac{(-1)^{\mu_i}}{\mu_i! \lambda_i^{\mu_k}}. \tag{D9}$$

We define by convention $Q_0 := 1$.

Note that $\sum_{\boldsymbol{\lambda}\vdash m} |\xi_{\boldsymbol{\lambda}}| = m!$ since $\xi_{\boldsymbol{\lambda}}$ counts (with sign) the number of permutations of m elements of cycle type $\boldsymbol{\lambda}$. In addition, we remark that the number of partitions $p(m)$ of a given integer m scales as $\log p(m) \sim C\sqrt{m}$, where C is a universal constant. This makes the sum in equation (8) prohibitive to evaluate already for modestly large values of m. However, as shown in section 4.3, it is possible to efficiently compute $Q_m(\boldsymbol{z})$ without splitting it into its different summands.

Definition 2. We define $P(X)$ to be

$$P(X) := \sum_{m=0}^{n} \frac{n!}{m!} Q_m(\boldsymbol{z}) X^{n-m}. \tag{D10}$$

Now that we know how to obtain the $\boldsymbol{x}$ that satisfy $\boldsymbol{z}$ in equation (32), let us turn to the system of equations that actually arises from equation (23). Note that equation (32) does not take into consideration the z_0 term, but by incorporating the condition that $A_0 \propto \mathbb{1}$ then the system of equations of interest becomes equation (33).

The system of equations equation (32) is also known the power sum ideal. Its reduced Groebner basis is found as the elimination ideal of the power sums.

Corollary 3. *The elimination ideal of the power sums gives the compatibility conditions on the weights d_k of equation (22) to be representable with a diagonal TI MPS of bond dimension $D < n$.*

Indeed, let us consider $n = 4$ and $D = 3$. The elimination ideal of the power sums of three variables and degree four is

$$\langle x_1 + x_2 + x_3 - z_1, x_1^2 + x_2^2 + x_3^2 - z_2, x_1^3 + x_2^3 + x_3^3 - z_3, x_1^4 + x_2^4 + x_3^4 - z_4\rangle \cap \mathbb{K}[z_1, z_2, z_3, z_4] = \langle q(z_1, z_2, z_3, z_4)\rangle, \tag{D11}$$

where

$$q(z_1, z_2, z_3, z_4) = z_1^4 - 6z_1^2 z_2 + 3z_2^2 + 8z_1 z_3 - 6z_4 \tag{D12}$$

Note that the compatibility polynomial in equation (D12) is precisely the same polynomial $Q_4(\boldsymbol{z})$ in the constant term of the univariate polynomial in equation (D6). Hence, all the symmetric Dicke states for which the $\boldsymbol{z}$ obtained from their d_k belongs to the elimination ideal of the power sums of D variables with degree n are representable as a diagonal TI MPS of the form $A_0 \propto \mathbb{1}$ and $A_1 = \mathrm{diag}(\boldsymbol{x})$.

Appendix E. Linear programming approach for Dicke-diagonal states

Let us see how we can now apply equation (9) in a more systematic way to determine that the states of the Dicke basis are the only ones in which corollary 1 applies.

Let us consider ρ as a rank-1 projector onto a quantum state of the form equation (22). In virtue of equation (8) we have (note that for qubits the partition of n is identified by a single number, therefore we write α instead of $\boldsymbol{\alpha}$)

$$\sigma_\beta^\alpha = \sum_{p=0}^{n-m} \sqrt{\frac{\binom{m}{\alpha}\binom{m}{\beta}}{\binom{n}{\alpha+p}\binom{n}{\beta+p}}} \binom{n-m}{p} d^*_{\alpha+p} d_{\beta+p}. \tag{E1}$$

- If we set $d_\alpha = \delta(\alpha - k)$ then we have

$$\sigma_\beta^\alpha = \delta(\alpha-\beta)\binom{n}{k}^{-1}\binom{m}{\alpha}\binom{n-m}{k-\alpha} I_{[0,n-m]}(k-\alpha), \tag{E2}$$

  where $I_S(x)$ is the indicator function, which evaluates to 1 if $x \in S$ and 0 otherwise. This allows us to write the set of equations for any basis Dicke state:

$$\sum_{p=0}^{n-m} \rho_{\beta+p}^{\alpha+p} \sqrt{\frac{\binom{m}{\alpha}\binom{m}{\beta}}{\binom{n}{\alpha+p}\binom{n}{\beta+p}}} \binom{n-m}{p} = \delta(\alpha-\beta)\binom{n}{k}^{-1}\binom{m}{\alpha}\binom{n-m}{k-\alpha} I_{[0,n-m]}(k-\alpha). \tag{E3}$$

- If we take $m = n - 1$, we recover the result of corollary 1 in the following way: since

$$\sigma = \binom{n}{k}^{-1} \sum_{\alpha=k-1}^{k} \binom{n-1}{\alpha} |\alpha\rangle\langle\alpha|, \tag{E4}$$

  the conditions of the SdP equation (9) can be now rewritten as

$$\sum_{p=0}^{1} \rho_{\beta+p}^{\alpha+p} \sqrt{\frac{\binom{n-1}{\alpha}\binom{n-1}{\beta}}{\binom{n}{\alpha+p}\binom{n}{\beta+p}}} \binom{1}{p} = \delta(\alpha-\beta)\binom{n-1}{\alpha}\binom{n}{k}^{-1} I_{[0,1]}(k-\alpha). \tag{E5}$$

  We note that the right-hand side of equation (E5) is zero if $\alpha > k$ or $\alpha < k-1$. In these cases, in the diagonal ($\alpha = \beta$) we have a condition of the form

$$\rho_\alpha^\alpha \xi_\alpha + \rho_{\alpha+1}^{\alpha+1}\xi_{\alpha+1} = 0, \tag{E6}$$

  for some $\xi_\alpha > 0$ that we do not need to write here explicitly. Now, the semidefinite positivity condition on ρ from the SdP equation (9) implies that the diagonal elements must be non-negative: $\rho_\alpha^\alpha \geqslant 0$. Hence, for all $\alpha \geqslant k+1$ and $\alpha \leqslant k-2$ we must have $\rho_\alpha^\alpha = \rho_{\alpha+1}^{\alpha+1} = 0$. The condition $\rho \succeq 0$ further implies that all the elements in the respective rows and columns must be zero. Therefore, the only non-zero element ρ_α^α left is ρ_k^k, which must be 1 in virtue of equation (E5).

- If we trace out two parties, i.e. we take $m = n - 2$, then a similar argument follows: we see that for $\alpha > k$ or $\alpha < k - 2$ we have a condition in the diagonal similar to the form of equation (E6)

$$\rho_{\alpha}^{\alpha}\xi_{\alpha} + \rho_{\alpha+1}^{\alpha+1}\xi_{\alpha+1} + \rho_{\alpha+2}^{\alpha+2}\xi_{\alpha+2} = 0. \tag{E7}$$

  Again, in equation (E7) we have a linear combination of $\rho_{\alpha+p}^{\alpha+p} \geqslant 0$ (because $\rho \succeq 0$) with strictly positive weights $\xi_{\alpha+p}^{\alpha+p} > 0$. This implies that $\rho_{\alpha}^{\alpha} = 0$ for $\alpha \neq k$, and a similar argument follows. However, one needs to be careful in counting the number of zero and non-zero equations: we need $n > 4$ for equation (E7) to exist. To this end, let us see the general case:
- If we trace out $n - m$ parties, then we generalize the last two points: for $\alpha > k$ or $\alpha < k - (n - m)$ the condition on the diagonal is

$$\sum_{p=0}^{n-m} \rho_{\alpha+p}^{\alpha+p}\xi_{\alpha+p} = 0, \tag{E8}$$

  which implies $\rho_{k+1+p}^{k+1+p} = \rho_{k-1-p}^{k-1-p} = 0$ for $p \geqslant 0$. This condition is nontrivial as long as the number of equations $(m - 1)$ is greater than the number of nonzero left hand sides $(n - m + 1)$, i.e. whenever $m > n/2$. Therefore, the condition $\rho \succeq 0$ implies that all the off-diagonal elements must be zero and therefore $\rho_k^k = 1$.
- Suppose we trace out $n - m$ parties. Then we have the following system of equations:

$$\begin{pmatrix} \binom{n-m}{0} & \binom{n-m}{1} & \cdots & \binom{n-m}{n-m} & \cdots & 0 \\ 0 & \binom{n-m}{0} & \cdots & \binom{n-m}{n-m-1} & \cdots & 0 \\ \vdots & \vdots & \ddots & \vdots & \ddots & \vdots \\ 0 & 0 & \cdots & \binom{n-m}{n-2m} & \cdots & \binom{n-m}{n-m} \end{pmatrix} \begin{pmatrix} x_0 \\ x_1 \\ \vdots \\ x_{n-m} \\ \vdots \\ x_n \end{pmatrix} = \begin{pmatrix} \binom{n-m}{k} I_{[0,n-m]}(k) \\ \binom{n-m}{k-1} I_{[0,n-m]}(k-1) \\ \vdots \\ \binom{n-m}{k-m} I_{[0,n-m]}(k-m) \end{pmatrix}, \tag{E9}$$

  where we have defined for simplicity $x_p := \rho_p^p \binom{n}{k} / \binom{n}{p}$. If $m > n/2$, there must necessarily be zeroes in the right-hand side of equation (E9).

The question about uniqueness of solutions of linear programs [106] and semidefinite programs [107, 108] is an intensive field of research, due to its connection to rigidity theory. For instance, the general solution to the uniqueness of equation (11) can be expressed via

Theorem 2 [107]. *If ρ is a max-rank solution of equation (11), and we write $\rho = L^\dagger L$, where $L \in \mathbb{C}^{r\times n}$, then ρ is the unique solution of equation (11) if, and only if, the kernel of the linear space spanned by $L^\dagger A_\beta^\alpha L$ is trivial.*

Corollary 4 [107]. *If all the solutions to equation (11) share the same rank, then the solution must be unique.*

ORCID iDs

Albert Aloy https://orcid.org/0000-0002-1401-0184
Matteo Fadel https://orcid.org/0000-0003-3653-0030
Jordi Tura https://orcid.org/0000-0002-6123-1422

References

[1] Stillinger F H 1995 *Mathematical Challenges from Theoretical/Computational Chemistry* (Washington, DC: National Academy Press)
[2] Klyachko A A 2006 Quantum marginal problem and *n*-representability *J. Phys.: Conf. Ser.* **36** 72–86
[3] Liu Y-K, Christandl M and Verstraete F 2007 Quantum computational complexity of the *N*-representability problem: QMA complete *Phys. Rev. Lett.* **98** 110503
[4] Kempe J and Regev O 2003 3-local Hamiltonian is QMA-complete *Quantum Info. Comput.* **3** 258–64
[5] Kempe J, Kitaev A and Regev O 2006 The complexity of the local Hamiltonian problem *SIAM J. Comput.* **35** 1070–97
[6] Aharonov D, Gottesman D, Irani S and Kempe J 2009 The power of quantum systems on a line *Commun. Math. Phys.* **287** 41–65
[7] Kitaev A Y 1995 Quantum measurements and the abelian stabilizer problem (arXiv:quant-ph/9511026v1)
[8] Poulin D and Wocjan P 2009 Preparing ground states of quantum many-body systems on a quantum computer *Phys. Rev. Lett.* **102** 130503
[9] Abrams D S and Lloyd S 1999 Quantum algorithm providing exponential speed increase for finding eigenvalues and eigenvectors *Phys. Rev. Lett.* **83** 5162–5
[10] Ge Y, Tura J and Cirac J I 2019 Faster ground state preparation and high-precision ground energy estimation with fewer qubits *J. Math. Phys.* **60** 022202

[11] Ruskai M B 1969 N-representability problem: conditions on geminals *Phys. Rev.* **183** 129–41
[12] Yukalov V I and Coleman A J 2000 *Reduced Density Matrices* (Berlin: Springer)
[13] Walter M, Doran B, Gross D and Christandl M 2013 Entanglement polytopes: multiparticle entanglement from single-particle information *Science* **340** 1205–8
[14] Klyachko A 2004 Quantum marginal problem and representations of the symmetric group (arXiv:quant-ph/0409113v1)
[15] Christandl M, Doran B, Kousidis S and Walter M 2014 Eigenvalue distributions of reduced density matrices *Commun. Math. Phys.* **332** 1–52
[16] Schilling C, Benavides-Riveros C L and Vrana P 2017 Reconstructing quantum states from single-party information *Phys. Rev.* A **96** 052312
[17] Huber F 2017 Quantum states and their marginals: from multipartite entanglement to quantum error-correcting codes *PhD Thesis* Universität Siegen
[18] Wyderka N, Huber F and Gühne O 2017 Almost all four-particle pure states are determined by their two-body marginals *Phys. Rev.* A **96** 010102
[19] Gidofalvi G and Mazziotti D A 2004 Boson correlation energies via variational minimization with the two-particle reduced density matrix: exact N-representability conditions for harmonic interactions *Phys. Rev.* A **69** 042511
[20] Beste A, Runge K and Bartlett R 2002 Ensuring N-representability: Coleman's algorithm *Chem. Phys. Lett.* **355** 263–9
[21] Mazziotti D A 2012 Structure of fermionic density matrices: complete N-representability conditions *Phys. Rev. Lett.* **108** 263002
[22] Navascues M, Baccari F and Acin A 2020 Entanglement marginal problems (arXiv:2006.09064v2)
[23] Yu X-D, Simnacher T, Wyderka N, Chau Nguyen H and Gühne O 2020 Complete hierarchy for the quantum marginal problem (arXiv:2008.02124v1)
[24] Kim I H 2020 Entropy scaling law and the quantum marginal problem (arXiv:2010.07424v1)
[25] Gnutzmann S, Haake F and Kus M 1999 Quantum chaos of SU3 observables *J. Phys. A: Math. Gen.* **33** 143–61
[26] Wei T-C, Mosca M and Nayak A 2010 Interacting boson problems can be QMA hard *Phys. Rev. Lett.* **104** 040501
[27] Lipkin H J, Meshkov N and Glick A J 1965 Validity of many-body approximation methods for a solvable model *Nucl. Phys.* **62** 188–98
[28] Meshkov N, Glick A J and Lipkin H J 1965 Validity of many-body approximation methods for a solvable model *Nucl. Phys.* **62** 199–210
[29] Glick A J, Lipkin H J and Meshkov N 1965 Validity of many-body approximation methods for a solvable model *Nucl. Phys.* **62** 211–24
[30] Tura J, Augusiak R, Sainz A B, Vértesi T, Lewenstein M and Acín A 2014 Detecting nonlocality in many-body quantum states *Science* **344** 1256–8
[31] Schmied R, Bancal J-D, Allard B, Fadel M, Scarani V, Treutlein P and Sangouard N 2016 Bell correlations in a Bose–Einstein condensate *Science* **352** 441–4
[32] Tura J, Augusiak R, Sainz A B, Lücke B, Klempt C, Lewenstein M and Acín A 2015 Nonlocality in many-body quantum systems detected with two-body correlators *Ann. Phys., NY* **362** 370–423
[33] Aloy A 2020 Exploring quantum many-body systems from an entanglement and nonlocality perspective *Ph.D. Thesis* Universitat Politècnica de Catalunya
[34] Eckert K, Schliemann J, Bruß D and Lewenstein M 2002 Quantum correlations in systems of indistinguishable particles *Ann. Phys., NY* **299** 88–127
[35] Dicke R H 1954 Coherence in spontaneous radiation processes *Phys. Rev.* **93** 99–110
[36] Wieczorek W, Krischek R, Kiesel N, Michelberger P, Tóth G and Weinfurter H 2009 Experimental entanglement of a six-photon symmetric Dicke state *Phys. Rev. Lett.* **103** 020504
[37] Lücke B, Peise J, Vitagliano G, Arlt J, Santos L, Tóth G and Klempt C 2014 Detecting multiparticle entanglement of Dicke states *Phys. Rev. Lett.* **112** 155304
[38] McConnell R, Zhang H, Hu J, Ćuk S and Vuletić V 2015 Entanglement with negative wigner function of almost 3000 atoms heralded by one photon *Nature* **519** 439–42
[39] Tura J, Augusiak R, Hyllus P, Kuś M, Samsonowicz J and Lewenstein M 2012 Four-qubit entangled symmetric states with positive partial transpositions *Phys. Rev.* A **85** 060302
[40] Augusiak R, Tura J, Samsonowicz J and Lewenstein M 2012 Entangled symmetric states of N qubits with all positive partial transpositions *Phys. Rev.* A **86** 042316
[41] Tura J, Aloy A, Quesada R, Lewenstein M and Sanpera A 2018 Separability of diagonal symmetric states: a quadratic conic optimization problem *Quantum* **2** 45
[42] Šupić I, Coladangelo A, Augusiak R and Acín A 2018 Self-testing multipartite entangled states through projections onto two systems *New J. Phys.* **20** 083041
[43] Fadel M 2017 Self-testing dicke states (arXiv:1707.01215v1)
[44] Oszmaniec M, Augusiak R, Gogolin C, Kołodyński J, Acín A and Lewenstein M 2016 Random Bosonic states for robust quantum metrology *Phys. Rev.* X **6** 041044
[45] Grigoriy Blekherman R T and Parrilo P A (ed) 2013 *Semidefinite Optimization and Convex Algebraic Geometry* (Philadelphia: Society for Industrial and Applied Mathematics)
[46] Tura J, De las Cuevas G, Augusiak R, Lewenstein M, Acín A and Cirac J I 2017 Energy as a detector of nonlocality of many-body spin systems *Phys. Rev.* X **7** 021005
[47] Latorre J I, Orús R, Rico E and Vidal J 2005 Entanglement entropy in the lipkin-meshkov-glick model *Phys. Rev.* A **71** 064101
[48] Barthel T, Dusuel S and Vidal J 2006 Entanglement entropy beyond the free case *Phys. Rev. Lett.* **97** 220402
[49] Vidal J, Dusuel S and Barthel T 2007 Entanglement entropy in collective models *J. Stat. Mech.* P01015
[50] Orús R 2008 Universal geometric entanglement close to quantum phase transitions *Phys. Rev. Lett.* **100** 130502
[51] Pan F and Draayer J P 1999 Analytical solutions for the LMG model *Phys. Lett.* B **451** 1–10
[52] Links J, Zhou H-Q, McKenzie R H and Gould M D 2003 Algebraic Bethe ansatz method for the exact calculation of energy spectra and form factors: applications to models of Bose Einstein condensates and metallic nanograins *J. Phys. A: Math. Gen.* **36** R63–R104
[53] Ribeiro P, Vidal J and Mosseri R 2008 Exact spectrum of the Lipkin–Meshkov–Glick model in the thermodynamic limit and finite-size corrections *Phys. Rev.* E **78** 021106
[54] Sturm J F 1999 Using sedumi 1.02, a matlab toolbox for optimization over symmetric cones *Optim. Methods Softw.* **11** 625–53
[55] Fadel M and Tura J 2018 Bell correlations at finite temperature *Quantum* **2** 107

[56] Koffel T, Lewenstein M and Tagliacozzo L 2012 Entanglement entropy for the long-range Ising chain in a transverse field *Phys. Rev. Lett.* **109** 267203
[57] Knap M, Kantian A, Giamarchi T, Bloch I, Lukin M D and Demler E 2013 Probing real-space and time-resolved correlation functions with many-body Ramsey interferometry *Phys. Rev. Lett.* **111** 147205
[58] Gabbrielli M, Lepori L and Pezzè L 2019 Multipartite-entanglement tomography of a quantum simulator *New J. Phys.* **21** 033039
[59] Piga A, Aloy A, Lewenstein M and Frérot I 2019 Bell correlations at Ising quantum critical points *Phys. Rev. Lett.* **123** 170604
[60] Toh K C, Todd M J, Tütüncü R H and Tutuncu R H 1998 Sdpt3—a matlab software package for semidefinite programming *Optim. Methods Softw.* **11** 545–81
[61] Crosswhite G M, Doherty A C and Vidal G 2008 Applying matrix product operators to model systems with long-range interactions *Phys. Rev.* B **78** 035116
[62] Fröwis F, Nebendahl V and Dür W 2010 Tensor operators: constructions and applications for long-range interaction systems *Phys. Rev.* A **81** 062337
[63] Brunner N, Cavalcanti D, Pironio S, Scarani V and Wehner S 2014 Bell nonlocality *Rev. Mod. Phys.* **86** 419–78
[64] Fadel M and Tura J 2017 Bounding the set of classical correlations of a many-body system *Phys. Rev. Lett.* **119** 230402
[65] Brugués J T 2017 *Characterizing Entanglement and Quantum Correlations Constrained by Symmetry* (Berlin: Springer)
[66] Tavakoli A, Rosset D and Renou M-O 2019 Enabling computation of correlation bounds for finite-dimensional quantum systems via symmetrization *Phys. Rev. Lett.* **122** 070501
[67] Orús R 2014 A practical introduction to tensor networks: matrix product states and projected entangled pair states *Ann. Phys., NY* **349** 117–58
[68] Perez-Garcia D, Verstraete F, Wolf M M and Cirac J I 2007 Matrix product state representations *Quantum Inf. Comput.* **7** 401–30
[69] Biamonte J and Bergholm V 2017 Tensor networks in a nutshell (arXiv:1708.00006v1)
[70] Sanz M, Wolf M M, Pérez-García D and Cirac J I 2009 Matrix product states: symmetries and two-body Hamiltonians *Phys. Rev.* A **79** 042308
[71] Sanz M, Braak D, Solano E and Egusquiza I L 2017 Entanglement classification with algebraic geometry *J. Phys. A: Math. Theor.* **50** 195303
[72] Sanz M, Egusquiza I L, Di Candia R, Saberi H, Lamata L and Solano E 2016 Entanglement classification with matrix product states *Sci. Rep.* **6** 30188
[73] Mayers D and Yao A 2004 Self testing quantum apparatus *Quantum Inf. Comput.* **4** 273–86
[74] Šupić I and Bowles J 2020 Self-testing of quantum systems: a review (arXiv:1904.10042v2)
[75] Yang T H and Navascués M 2013 Robust self-testing of unknown quantum systems into any entangled two-qubit states *Phys. Rev.* A **87** 050102
[76] Bamps C and Pironio S 2015 Sum-of-squares decompositions for a family of Clauser–Horne–Shimony–Holt-like inequalities and their application to self-testing *Phys. Rev.* A **91** 052111
[77] Kaniewski J 2016 Analytic and nearly optimal self-testing bounds for the Clauser–Horne–Shimony–Holt and Mermin inequalities *Phys. Rev. Lett.* **117** 070402
[78] Wang J *et al* 2018 Multidimensional quantum entanglement with large-scale integrated optics *Science* **360** 285–91
[79] Zhang W-H *et al* 2019 Experimental demonstration of robust self-testing for bipartite entangled states *npj Quantum Inf.* **5** 4
[80] Salavrakos A, Augusiak R, Tura J, Wittek P, Acín A and Pironio S 2017 Bell inequalities tailored to maximally entangled states *Phys. Rev. Lett.* **119** 040402
[81] Kaniewski J, Supic I, Tura J, Baccari F, Salavrakos A and Augusiak R 2020 Maximal nonlocality from maximal entanglement and mutually unbiased bases, and self-testing of two-qutrit quantum systems (arXiv:1807.03332v1)
[82] Šupić I, Augusiak R, Salavrakos A and Acín A 2016 Self-testing protocols based on the chained bell inequalities *New J. Phys.* **18** 035013
[83] Wu X, Cai Y, Yang T H, Le H N, Bancal J-D and Scarani V 2014 Robust self-testing of the three-qubit W state *Phys. Rev.* A **90** 042339
[84] Wu X 2016 Self-testing: walking on the boundary of the quantum set *PhD Thesis* National University of Singapore
[85] Li X, Cai Y, Han Y, Wen Q and Scarani V 2018 Self-testing using only marginal information *Phys. Rev.* A **98** 052331
[86] Baccari F, Augusiak R, Šupić I, Tura J and Acín A 2018 Scalable bell inequalities for qubit graph states and robust self-testing (arXiv:1812.10428v1)
[87] Augusiak R, Salavrakos A, Tura J and Acín A 2019 Bell inequalities tailored to the Greenberger–Horne–Zeilinger states of arbitrary local dimension (arXiv:1907.10116v1)
[88] Tura J, Sainz A B, Vértesi T, Acín A, Lewenstein M and Augusiak R 2014 Translationally invariant multipartite bell inequalities involving only two-body correlators *J. Phys. A: Math. Theor.* **47** 424024
[89] Scarani V 2012 The device-independent outlook on quantum physics *Acta Phys. Slovaca* **62** 347–409
[90] Baccari F, Tura J, Fadel M, Aloy A, Bancal J-D, Sangouard N, Lewenstein M, Acín A and Augusiak R 2019 Bell correlation depth in many-body systems *Phys. Rev.* A **100** 022121
[91] Aloy A, Tura J, Baccari F, Acín A, Lewenstein M and Augusiak R 2019 Device-independent witnesses of entanglement depth from two-body correlators *Phys. Rev. Lett.* **123** 100507
[92] Tura J, Aloy A, Baccari F, Acín A, Lewenstein M and Augusiak R 2019 Optimization of device-independent witnesses of entanglement depth from two-body correlators *Phys. Rev.* A **100** 032307
[93] Fadel M, Aloy A and Tura J 2020 Bounding the fidelity of quantum many-body states from partial information *Phys. Rev.* A **102** 020401
[94] Doherty A C, Parrilo P A and Spedalieri F M 2004 Complete family of separability criteria *Phys. Rev.* A **69** 022308
[95] Navascués M, Owari M and Plenio M B 2009 Power of symmetric extensions for entanglement detection *Phys. Rev.* A **80** 052306
[96] Tóth G and Gühne O 2009 Entanglement and permutational symmetry *Phys. Rev. Lett.* **102** 170503
[97] Bachoc C, Gijswijt D C, Schrijver A and Vallentin F 2011 Invariant semidefinite programs *Handbook on Semidefinite, Conic and Polynomial Optimization* (Berlin: Springer) pp 219–69
[98] Fadel M, Zibold T, Décamps B and Treutlein P 2018 Spatial entanglement patterns and Einstein–Podolsky–Rosen steering in bose-einstein condensates *Science* **360** 409–13
[99] Navascués M, Pironio S and Acín A 2008 A convergent hierarchy of semidefinite programs characterizing the set of quantum correlations *New J. Phys.* **10** 073013

[100] Cavalcanti D and Skrzypczyk P 2016 Quantum steering: a review with focus on semidefinite programming *Rep. Prog. Phys.* **80** 024001
[101] Jordan P and Wigner E 1928 ber das Paulische quivalenzverbot *Z. Phys.* **47** 631–51
[102] Dmitriev D V, Krivnov V Y, Ovchinnikov A A and Langari A 2002 One-dimensional anisotropic Heisenberg model in the transverse magnetic field *J. Exp. Theor. Phys.* **95** 538–49
[103] Alcaraz F C and Malvezzi A L 1995 Critical and off-critical properties of the XXZ chain in external homogeneous and staggered magnetic fields *J. Phys. A: Math. Gen.* **28** 1521–34
[104] Zhou J, Hu Y, Zou X-B and Guo G-C 2011 Ground-state preparation of arbitrarily multipartite dicke states in the one-dimensional ferromagnetic spin-12 chain *Phys. Rev.* A **84** 042324
[105] Meredith D C, Koonin S E and Zirnbauer M R 1988 Quantum chaos in a schematic shell model *Phys. Rev.* A **37** 3499–513
[106] Mangasarian O L 1984 Normal solutions of linear programs *Mathematical Programming Studies* (Berlin: Springer) pp 206–16
[107] Zhu Z, Man-Cho So A and Ye Y 2010 Universal rigidity: towards accurate and efficient localization of wireless networks *2010 Proc. IEEE INFOCOM* (IEEE)
[108] Alfakih A Y 2007 On dimensional rigidity of bar-and-joint frameworks *Discrete Appl. Math.* **155** 1244–53